https://doi.org/10.5194/wcd-2020-1
Preprint. Discussion started: 14 January 2020

The role of large-scale dynamics in an exceptional sequence of severe thunderstorms in Europe May/June 2018

Susanna Mohr[1,2], Jannik Wilhelm[1], Jan Wandel[1], Michael Kunz[1,2], Raphael Portmann[3], Heinz Jürgen Punge[1], Manuel Schmidberger[1], and Christian M. Grams[1]

[1]Karlsruhe Institute of Technology (KIT), Institute of Meteorology and Climate Research (IMK-TRO), Karlsruhe, Germany
[2]Center for Disaster Management and Risk Reduction Technology (CEDIM), Karlsruhe, Germany
[3]Institute for Atmospheric and Climate Science, ETH Zurich, Switzerland

Correspondence: Susanna Mohr (mohr@kit.edu)

Abstract. Over three weeks in May and June 2018, an exceptionally large number of thunderstorms hit vast parts of western and central Europe, causing precipitation of up to 80 mm and several flash floods. During this time, the large-scale atmospheric circulation, which was characterized by a blocking situation over northern Europe, influenced atmospheric conditions relevant for thunderstorm development. Initially, the southwesterly flow on the western flank of the blocking anticyclone induced the advection of warm, moist, and unstably stratified air masses. Due to a low-pressure gradient associated with the blocking anticyclone, these air masses were trapped in western and central Europe, remained almost stationary and prevented a significant air mass exchange. In addition, the low-pressure gradient led to weak flow conditions in the mid-troposphere and thus to low vertical wind shear that prevented thunderstorms from developing into severe organized systems. Most of the storms formed as local-scale, relatively slow-moving single cells. However, due to the related weak propagation speed, several thunderstorms were able to produce torrential heavy rain that affected local-scale areas and triggered several flash floods.

Atmospheric blocking also increased the upper-level cut-off low frequency on its upstream regions, which was up to 10 times higher than the climatological mean. Together with filaments of positive potential vorticity (PV), the cut-offs served as trigger mechanisms for a majority of the thunderstorms. For the 22-day study period, we found that more than 50 % of lightning strikes can be linked to a nearby cut-off low or PV filament. The exceptional persistence of low stability combined with weak wind speed in the mid-troposphere over three weeks has not been observed during the past 30 years.

Keywords: Europe, thunderstorms, severe convective storms, heavy rain, flash floods, atmospheric blocking, weather regimes, cut-off lows, potential vorticity

1 Introduction

Historically, the period from May to mid of June 2018 has been among the most active periods of severe convective storms associated with heavy rain, hail, convective wind gusts and even tornadoes over large parts of western and central Europe. More than 1,500 reports of hazardous weather events were documented by the European Severe Weather Database (ESWD; Dotzek et al., 2009). Rainfall totals of up to 90 mm within a few hours caused (pluvial) flash floods in various municipalities. Gust speeds of up to 30 m s^{-1} led to numerous fallen trees and severely damaged buildings. For example, from 26 May to 1 June

https://doi.org/10.5194/wcd-2020-1
Preprint. Discussion started: 14 January 2020

2018, thunderstorms caused insured (overall) losses of about 300 (430) million USD according to Munich Re's NatCatSERVICE. It was the costliest convective storm event in western Europe that year (Munich Re, 2019).

In general, the development of convective storms results from scale interactions of different processes in the atmosphere. Whereas thunderstorms initiate from positively buoyant and thus freely rising air parcels on the local-scale (micro-α according to Orlanski, 1975), triggering mechanisms occur over a wide range of scales. For example, lifting mechanisms on the mesoscale include orographic lifting, horizontal convective rolls, or gravity waves (Wilson and Schreiber, 1986; Banacos and Schultz, 2005; Barthlott et al., 2010), whereas large-scale lifting is related to cold fronts, drylines, or sea-breeze fronts (e.g., Doswell, 1987; Schemm et al., 2016; Soderholm et al., 2017; Kunz et al., 2018, 2020). In addition, the general setting conducive for convective activity, i.e. the prevailing thermodynamical and dynamical conditions, is controlled by processes on the synoptic scale and beyond. Several authors have found a relation between thunderstorm probability and various teleconnection patterns (e.g., North Atlantic Oscillation, Madden-Julian Oscillation, El Niño-Southern Oscillation; Giaiotti et al., 2003; Barrett and Gensini, 2013; Allen and Karoly, 2014; Allen et al., 2015; Piper et al., 2019). All these mechanisms may operate individually or in tandem, and may directly trigger convection if they are strong enough or — in addition to the daily temperature cycle — serve the precondition of the thermodynamic environment.

In this study, the general synoptic situation during the thunderstorm episode was similar to that prevailing over a 15-day period in May/June 2016, where an exceptionally large number of thunderstorms caused several flash floods, primarily in Germany (Piper et al., 2016, hereinafter referred to as PIP16). Throughout this period, a blocking anticyclone over the North Sea and Scandinavian region prevented an exchange of the dominant unstably stratified air masses over several days. In addition, low wind speeds throughout the troposphere caused the thunderstorms to be almost stationary with the effect of torrential rain accumulations in several small regions.

Atmospheric blocking, with a typical lifetime of several days to weeks, is a quasi-stationary, persistent flow situation that modulates the large-scale extratropical circulation (Rex, 1950a, b; Barriopedro et al., 2006; Woollings et al., 2018). Such blocks typically occur either in a *dipole configuration* with an accompanying cut-off low on the equatorward side (Rex, 1950a; Tibaldi and Molteni, 1990) or they adopt an *omega-shape* with cut-off lows forming at the flanks of the blocked region (Dole and Gordon, 1983). At first, the relationship between blocking and convective activity seems counterintuitive because heatwaves and associated droughts are frequently associated with such patterns (e.g., Pfahl and Wernli, 2012; Bieli et al., 2015; Schaller et al., 2018; Röthlisberger and Martius, 2019), but in peripheral locations upstream and downstream blocks can also create environmental conditions conducive for convection development (PIP16; Mohr et al., 2019).

In the potential vorticity (PV) framework, a cut-off low is an upper-level closed anomaly of stratospheric high PV air (e.g., Wernli and Sprenger, 2007; Nieto et al., 2007a, 2008). PV anomalies, in general, have a far-field impact on the meteorological conditions in their surroundings (cf. Hoskins et al., 1985). Below the positive PV anomaly, isentropes bend upward, resulting in reduced static stability and increased lifting. Due to an induced cyclonic circulation anomaly, the positive PV anomaly favours isentropic gliding up and thus ascent along the isentropes that usually bend upward towards the pole. Finally, when the positive PV anomaly propagates, air masses ascend isentropically at the PV anomalies' upstream side. These three mechanisms associated with lifting are intrinsic to upper-level positive PV anomalies in general. At the flanks of a mature PV cut-off, small meso-scale filaments of positive PV often separate and are advected away, particularly when the PV cut-off gradually decays (Portmann et al., 2018). When such a positive PV filament moves over air masses that are conditionally or potentially unstably stratified, they trigger lifting and thereby effectively release convective available potential energy and facilitate/cause deep moist convection (cf. Grams and Blumer, 2015).

A connection between atmospheric blocking and heavy precipitation events has already been established – especially for flood events (e.g., Martius et al., 2013; Grams et al., 2014; Piaget et al., 2015; Sousa et al., 2017; Lenggenhager et al., 2018; Lenggenhager and Martius, 2019). A recent study by Tarabukina et al. (2019) shows a correlation between the annual variation of summer lightning activity in Yakutia (Russia) and the frequency of atmospheric blocking in Western Siberia. Mohr et al. (2019) also demonstrate a relationship between convective activity and specific blocking situations but in the European sector. They found a block over the Baltic Sea frequently associated with increased thunderstorm occurrences because of southwesterly advection of warm, moist and unstable air masses on its western flank. In addition, such situations are usually associated with weak wind speeds at mid-tropospheric levels (cf. PIP16), so that thunderstorms become almost stationary and usually do not develop into organized structures such as large mesoscale convective systems or supercells.

The primary objective of this paper is to examine the conditions and processes that made this particular thunderstorm episode unique. We focus on the process interaction across scales, i.e., from the large-scale dynamics such as blocking and convection triggered by cut-off lows and/or PV filaments to modifications of the convective environment to local-scale thunderstorm occurrences. Further objectives are to highlight the synoptic setting during the thunderstorm episode, to estimate the severity of the events, and to place the thunderstorm episode in a historical context.

The paper is structured as follows: Section 2 presents the different data sets and the methods used. Section 3 discusses the large-scale conditions including a detailed event description. In Section 4, we investigate the role of PV cut-off on the development of deep moist convection. Section 5 puts the results in a historical context. Finally, Section 6 and Section 7 discuss and summarize the main results and draws conclusions.

2 Data and methods

The study area includes parts of central and western Europe – France, Benelux (Belgium, Netherlands, Luxembourg), Germany, Switzerland and Austria (see Fig. 1) – for which data were available. The study period extends over three weeks from 22 May to 12 June 2018, where most of the thunderstorms and secondary effects occurred (see Sect. 3.1). For some investigations, we considered an extended study period from 1 May to 20 June 2018. For the purpose of climatological comparison, the 30-year period from 1981 to 2010 (May/June) was the reference period (unless otherwise indicated).

https://doi.org/10.5194/wcd-2020-1
Preprint. Discussion started: 14 January 2020

2.1 Observation data

2.1.1 ESWD reports

Reports about heavy rain, hail (diameter $\geqslant 2\,\mathrm{cm}$), and convective wind gusts $\geqslant 25\,\mathrm{m\,s^{-1}}$ are collected by the European Severe Weather Database (ESWD; Dotzek et al., 2009; Groenemeijer et al., 2017). The ESWD is a step-by-step quality controlled (four levels) database providing detailed information about severe convective storms in Europe, mainly based on storm chasers, eyewitnesses, voluntary observers, meteorological services, and newspaper reports. Using a homogeneous data format, these observations contain information about hazardous weather events such as location, time, intensity, and damage-related information. For a detailed description of the event reporting criteria see ESSL (2014).

2.1.2 Precipitation totals

Daily precipitation totals of 232 stations distributed across the domain (41°N – 58°N 4°W – 20°E) were collected from the European Climate Assessment and Dataset (ECA&D), a database of daily meteorological station observations across Europe (Klein Tank et al., 2002). In addition, hourly and daily data were obtained from the Météo-France (1223 stations with hourly data / 1935 stations with daily data), the Royal Netherlands Meteorological Institute (KNMI; 50/322), the German Weather Service (DWD; 958/810), MeteoSwiss (952/0), and the Central Institution for Meteorology and Geodynamics (ZMAG; 254/0) – the national weather services of those countries with the highest count of flash flood reports (see Fig. 1). For statistics of hourly and 3-hour extreme rainfall events, we applied the same severity thresholds used in the ESWD (ESSL, 2014), which amount to 35 and 60 mm, respectively (Wussow, 1922; Nachtnebel, 2003). Note that the 24-hour criterion of 170 mm was not measured at any of the stations.

To put the rainfall of the 2018 thunderstorm episode in a historical context, we estimate return periods of single heavy precipitation events based on regionalized precipitation data (*REGionalisierte NIEderschläge*, REGNIE) provided by DWD (DWD, 2018). REGNIE is a gridded data set of 24-hour totals (from 06 UTC to 06 UTC on the next day) based on several thousand climate stations more or less evenly distributed across Germany (the so-called RR collective). The REGNIE algorithm interpolates the measurement data to a regular grid of $1\,\mathrm{km}^2$ considering altitude, exposure, and climatology (Rauthe et al., 2013). The data have been available since 1951 but cover only Germany. Note that the REGNIE time series are affected by temporal changes in the number of rain gauges considered by the regionalization. For our purpose, the homogeneity of the data are sufficient.

Statistical return periods of REGNIE totals during the study period are quantified using the Generalized Extreme Value (GEV) distribution (e.g., Beniston et al., 2007; van den Besselaar et al., 2013; Schröter et al., 2015; Ehmele and Kunz, 2018). The Fisher-Tippett Type I distribution, also known as the Gumbel distribution (Wilks, 2006) with the cumulative distribution function (CDF) is widely used and appropriate for precipitation statistics

$$F(R) = \exp\left[-\exp\left(\frac{\zeta - R}{\beta}\right)\right], \qquad (1)$$

https://doi.org/10.5194/wcd-2020-1
Preprint. Discussion started: 14 January 2020

with ζ and β as location and scale parameters. For their estimation, we used the Method of Moments and considered the 67-year period from 1951 to 2017 (summer half-year from April to September):

$$\beta = \frac{\sigma\sqrt{6}}{\pi} \qquad \& \qquad \zeta = \bar{R} - \delta \cdot \beta\,, \tag{2}$$

with σ as the standard derivation, $\bar{R}$ as the mean of the REGNIE sample and δ as the Euler-Mascheroni constant (≈ 0.5772). The return period t_{RP} is directly related to the probability of occurrence of the threshold $P(R \geqslant R_{trs}) = t_{RP}^{-1}$ so that the CDF is given by $F(R) = 1 - t_{RP}^{-1}$. The resulting equation to estimate the return period t_{RP} is:

$$t_{RP}(R) = \left[1 - \exp\left(-\exp\left(\frac{\zeta - R}{\beta}\right)\right)\right]^{-1}. \tag{3}$$

2.1.3 Lightning data

Lightning data are obtained from the ground-based low-frequency lightning detection system of Siemens part of the EUCLID network (EUropean Cooperation for LIghtning Detection; Drüe et al., 2007; Schulz et al., 2016; Poelman et al., 2016). Available for the whole study domain, the data are projected on an equidistant grid of 10×10 km^2 and accumulated over 6-hour periods centered around the times in ERA-Interim (e.g., for the 06 UTC reanalysis the lightning period is 03 – 09 UTC). We consider all types of flashes including cloud-to-ground, cloud-to-cloud, and intra-cloud flashes, whereas polarity or peak current are not investigated.

2.1.4 Sounding stations

Atmospheric conditions are estimated from vertical profiles of temperature, moisture, and wind speed/direction at seven sounding stations provided by DWD and the Integrated Global Radiosonde Archive (IGRA) from the National Climatic Data Center (Durre et al., 2006). These stations are distributed over the entire domain: Bordeaux (44.83°N 0.68°W) and Trappes (48.77°N 2.00°E) in France; Essen (51.41°N 6.97°E), Stuttgart (48.83°N 9.20°E), and Munich (48.24°N 11.55°E) in Germany; Payerne (46.82°N 6.95°E) in Switzerland, and Vienna (48.23°N 16.37°E) in Austria (see Fig. 1). Other sounding stations could not be used because of multiple gaps in the time series. We use all variables at 12 UTC because thunderstorms in central Europe usually peak during the late afternoon (Wapler, 2013; Poelman et al., 2016; Piper and Kunz, 2017).

Atmospheric stability is estimated from the surface-based Lifted Index (SLI; Galway, 1956), which has been identified in several studies as the parameter with the best representation of convective environmental conditions in central Europe (e.g., Haklander and van Delden, 2003; Manzato, 2003; Kunz, 2007; Mohr and Kunz, 2013; Rädler et al., 2018).

2.1.5 Storm tracks computed from radar reflectivity

Storm motion vectors are computed from three-dimensional (3D) radar reflectivity data from the radar network of DWD. The data, which includes 17 radar stations with dual-polarization Doppler radars, are combined and interpolated into a radar composite with a spatial resolution of 1×1 km^2 (Cartesian grid). The temporal resolution of the individual scans is 15 minutes. Radar reflectivity is available on 12 equidistant vertical levels with a distance of 1 km. For the whole period between 2005 and

https://doi.org/10.5194/wcd-2020-1
Preprint. Discussion started: 14 January 2020

2018, which is used to relate the storm motions computed for the investigation period to the climatology (Sect. 5.1), data were stored in six reflectivity classes only. The two highest classes, which are considered here, range from 46 to 55 dBZ and ⩾ 55 dBZ.

To identify storm tracks, the cell-tracking algorithm TRACE3D (Handwerker, 2002) was adapted to the DWD radar composite in Cartesian coordinates. Once the algorithm detects a severe convective cell, the cell can be re-detected in the consecutive time steps and thus merged into a cell track. For this study, only severe convective storms frequently associated with hazardous weather are considered; thus storms were defined by having a minimum reflectivity of 55 dBZ (corresponding to the highest class) and a vertical extension of at least 1 km. Based on TRACE3D, information about width, length, duration, and propagation speed, as well as direction, is available for each individual thunderstorm track. More details about data and the tracking method can be found in Puskeiler et al. (2016) and Schmidberger (2018). Due to a lack of 3D radar data for France in 2018, our investigation refers only to severe convective storms that occurred in Germany.

2.2 Model data

We use the European Centre for Medium-Range Weather Forecasts (ECMWF) high-resolution operational analysis data and ECMWF ERA-Interim reanalysis (Dee et al., 2011) to describe the large-scale meteorological conditions and to identify both weather regimes (see Sect. 2.3) and cut-off lows (see Sect. 2.4). ECMWF analysis is available 6-hourly interpolated to a regular grid with 0.125° horizontal resolution. ERA-Interim used for the historical analysis is available 6-hourly interpolated to a regular grid at 1.0° horizontal resolution.

2.3 North Atlantic-European weather regimes

The large-scale flow conditions in the Atlantic-European region are characterized in terms of a definition of seven year-round weather regimes based on 10-day low-pass-filtered 500 hPa geopotential height anomalies (Z500'; Grams et al., 2017). The regimes are identified by k-means clustering in the phase-space spanned by the seven leading empirical orthogonal functions (EOFs). Based on these seven clusters, an active weather regime life-cycle is derived from the normalized projection of each 6-hourly anomaly in the cluster mean following Michel and Rivière (2011). Thereby, time steps with weak projections are filtered out (no regime). An active regime life-cycle persists for at least 5 days but fulfills further criteria as described in Grams et al. (2017).

Our weather regime definition is in line with 'classical' concepts of four seasonal regimes for Europe (e.g. Vautard, 1990; Michelangeli et al., 1995; Ferranti et al., 2015), but reflects important seasonal differences. Three of the seven regimes are dominated by a negative Z500' and enhanced cyclonic activity. These are the *Atlantic Trough (AT)* regime with a trough extending towards western Europe, the *Zonal regime (ZO)* with cyclonic activity around Iceland, and the *Scandinavian Trough (ScTr)* regime with a trough shifted towards the east. The remaining four regimes are characterized by a positive Z500' centered at different locations and therefore referred to as 'blocked regimes'. These are the *Atlantic Ridge (AR)* regime, with a blocking ridge over the eastern North Atlantic and an accompanying trough extending from eastern Europe into the central Mediterranean, the *European Blocking (EuBL)* regime, with a blocking anticyclone extending from Western Europe to the North Sea, *Scandinavian Blocking (ScBL)*, with high-latitude blocking over Scandinavia, and *Greenland Blocking (GL)* with a blocking ridge over the Greenland-Icelandic region.

2.4 Identification of PV cut-off and matching with lightning data

We identify upper-level cut-off lows based on PV on the 325 K isentropic surface from ERA-Interim using the algorithm of Wernli and Sprenger (2007) and Sprenger et al. (2017). The optimal level for the inspection of weather systems on isentropic surfaces depends on the season. The specific level of 325 K used here is motivated by the literature (cf. Röthlisberger et al., 2018) and the inspection of isentropic PV charts for our case. The algorithm searches for closed areas of PV larger than 2 PVU, which are disconnected from the main PV reservoir that expands across the North Pole.

The identified PV cut-offs are then related to thunderstorm events using lightning data on the $10 \times 10\,\mathrm{km}^2$ grid cells. We utilize the smallest distance approach to link a grid cell in the lightning data set to a grid point in the PV cut-off data set. The different grid sizes between the model and observation data sets require matching multiple grid cells (lightning data) to one PV cut-off grid point. This means if a grid point shows the presence of a PV cut-off, all flashes from the associated grid cells are linked to it.

To account for the far-field impact of lifting and destabilization by a PV cut-off, we expand the PV cut-off mask by a buffer. This scale is estimated from the typical Rossby radius of deformation

$$L_R = \frac{N \cdot H}{f_0} \tag{4}$$

associated with a PV cut-off. Here, N is the Brunt-Väisälä frequency, H is the scale height, and f_0 is the Coriolis parameter. For characteristic values in mid-latitudes with $N = 0.01\,\mathrm{s}^{-1}$ and $f_0 = 10^{-4}\,\mathrm{s}^{-1}$, N/f_0 is typically in the order of 100. A scale height of 10 km leads to a Rossby deformation radius of 1,000 km, which is typical for synoptic scales. We assume that some of the PV cut-offs during the study period have a vertical extent of fewer than 10 km. Therefore, we chose a conservative deformation radius (buffer) of about 500 km. The robustness of the chosen deformation radius is investigated both qualitatively and quantitatively. We found that a change in the radius of 100 km, for example, leads to an increase or decrease of 10 % in the total amount of lightning strikes associated with a PV cut-off during our study period. Such small changes do not affect the qualitative interpretation of our results.

2.5 Persistence analysis

Days with constant atmospheric conditions tend to form temporal clusters of certain weather events (here thunderstorms) with a lifetime of several days. This behavior can be described statistically by the concept of persistence. The persistence or the cluster length n of a specified event is defined as the sequence of days (between 1 and x days) with the binary parameter with values of 1 (event day = criterion fulfilled) or zero (non-event day = criterion not fulfilled). Within a cluster of seven event days, we allow one day to be a non-event one (skip day), which is not considered in the total length n. For more information on the concept see PIP16.

In the study, we investigate the co-occurrence of low stability (using the SLI) and low mid-tropospheric wind speeds (using the horizontal wind speed in 500 hPa, v_{500hPa}). For this purpose, the same thresholds are chosen as in PIP16. We use the basic criterion TH_{BC}, which is fulfilled if both conditions apply: SLI < 0 K and $v_{500hPa} < 10\,\mathrm{m\,s^{-1}}$. In addition, we also discuss our results in context with the strict criterion (TH_{SC}), which is fulfilled with SLI < -1.3 K and $v_{500hPa} < 8\,\mathrm{m\,s^{-1}}$.

3 Description of the thunderstorm episode

3.1 Overview

The period from May to mid-June 2018 was characterized by a large number of thunderstorms that spread across the study area, several of which were associated with heavy rainfall, hail, and strong wind gusts (Fig. 2a). More than 1,500 severe weather reports were collected and archived by the ESWD in our study area during that period. Lightning strikes were recorded on each day, and the affected area ranges between 100 $\mathrm{km^2}$ on 19 June and 1,100,000 $\mathrm{km^2}$ on 29 May (accumulations of the $10 \times 10\,\mathrm{km^2}$ grids).

The three-week period from 22 May until 12 June was the most active thunderstorm episode with a total of 868 heavy rain, 144 hail, and 145 convective wind gust reports based on the ESWD. An average area of 715,000 $\mathrm{km^2}$ was affected by lightning per day, indicating that several thunderstorm developments spread over the entire investigation area. The extraordinarily large number of thunderstorms, several of them severe, and the unusual persistence of that situation over three weeks motivated us to select that time frame as the study period.

As shown in Figure 2b, most of the severe weather reports came from the western part of France, Benelux, central and southern Germany, and the easternmost part of Austria. At the beginning of the study period, central Europe was particularly affected. On 22 May, thunderstorms associated with heavy rainfall and small hail with diameters of around 2 cm were restricted to Benelux and western Germany. Some entries report on flash floods and mudslides, for example in the Heilbronn area (SW Germany). Two days later, on 24 May, the federal state of Saxony (east Germany), the east of Austria, and parts of Belgium were hit by torrential rain accumulations. The German station Bad Elster-Sohl in Saxony (see Fig. 1) on the border to the Czech Republic, for example, measured a record of 86.3 mm / 3 h and 154.9 mm / 24 h (Table 1). On 26 May, several wind reports with gust speeds of up to 29 $\mathrm{m\,s^{-1}}$ (Poitiers, France; see Fig. 1) and hail reports indicating hailstones with a diameter of up to 5 cm were recorded, particularly in the French coastal region of the Bay of Biscay.

The subsequent time frame from 27 May to 1 June was the most active both in terms of the area affected by lightning and the number of ESWD reports (Fig. 2a). Widespread thunderstorms were observed mainly in Benelux, Germany, and France, but also sporadically in Switzerland and Austria (see discussion below in Sect. 4), all of them associated with large rain accumulations and subsequent flooding, hail between 2 and 4 cm in diameter, and damaging wind reports. Many of the record-breaking rain totals recorded during one and three hours, respectively, occurred within this period (see next Sect. 3.2). The highest number of ESWD reports (150) was issued on 29 May, followed by 31 May, most of them reporting heavy rainfall leading to a couple of flash floods and landslides, which destroyed buildings, vehicles, streets and even railway tracks.

https://doi.org/10.5194/wcd-2020-1
Preprint. Discussion started: 14 January 2020

In the first half of June, damaging hail (up to 5 cm) and heavy rainfall were still reported almost daily somewhere in the study domain, though less frequently than before. Also, the area affected by lightning shows a decrease by 7 June. Towards the end of the study period, convective activity increased again. Especially on the last day of the study period, on 12 June, the proportion of gust reports indicating wind speeds between 25 and 31 m s^{-1} to all reports was very large.

After the convectively most active period, when environmental conditions became more stable, thunderstorms rarely occurred (cf. Sect. 3.3). The area affected by lightning decreased considerably and no further severe weather reports were archived in the ESWD.

3.2 Rainfall statistics

As adumbrated in the previous section, heavy rain in May and June, especially during the study period, was a striking phenomenon, chiefly because of the low wind speed and the associated slow propagation of the thunderstorms. Figure 3 shows the time series of the frequencies of hourly (1 h) and 3-hour (3 h) rain gauge measurements exceeding the ESWD heavy rain criteria of 35 mm and 60 mm, respectively. The 1 h criterion was fulfilled during the study period in sum 167 times (Fig. 3a) with an average of about 7.6 stations per day with a variability between one and 20 stations, the latter on the day with the second most ESWD severe weather reports (cf. Sect. 3.1). The 3 h criterion was reached 38 times, with a maximum of at least 5 stations on three days (Fig. 3c). The strength and spatial extent of the lifting forcing varied from day to day, which explains the fluctuations of daily heavy rain frequencies. The location of the respective stations shows heavy rain events in all of the countries under consideration without any clustering (Fig. 3b,d). A few outstanding events are described below.

A conspicuously high 1 h rain sum of 85.7 mm was measured at Dietenhofen close to Nuremberg in the south of Germany on 31 May (Table 1 and Fig. 3b), also listed high in the ranking of highest 3 h rain sums. Similarly high 3 h values have been gauged in Prades-le-Lez in southern France on 11 June, Puchberg am Schneeberg in eastern Austria on 12 June and the above mentioned station Bad Elster-Sohl in eastern Germany on 24 May (see locations in Fig. 1). At the latter station, the extremely high 24 h total of 154.9 mm was caused by a slightly multicellular organized and very slow-moving convective system that was elongated in the propagation direction. Due to that configuration, the station Bad Elster-Sohl was hit successively by several embedded individual cell cores of the entire cluster. Several streets and buildings were flooded and a barrage dam over-flowed.

One week later, in the evening hours of 31 May, a similarly slow northwest-moving multicellular system formed along a convergence zone in northeastern France and southwestern Germany. This day exhibited the highest number of stations (20) with 1 h precipitation totals of more than 35 mm (Fig. 3a), appears four times in the top list of 1 h precipitation totals in Table 1, and also had more than 110 heavy rain reports in the ESWD (Fig. 2a). Another exceptional example is the last day of the study period, 12 June, were in addition to the high number of gust reports mentioned above, five of the nine highest 24 h rain totals occurred (cf. Table 1). In southwestern France and the Alps including its surroundings, continuous rain with regionally strong embedded convection occurred, as more stable air masses poured in the west and central Europe from the northwest.

3.3 Environmental conditions

3.3.1 Synoptic overview

In the first week of May 2018, a large-scale mid-tropospheric area of high geopotential stretched out from the Azores over central Europe and the Baltic to western Russia (Fig. 4a), attended by a corresponding prolonged lower-level high-pressure system (not shown). This configuration was associated with the advection of warm and relatively dry air masses over large parts of Europe. In the second week of May, the pattern transitioned into a blocked situation over Europe (see also Sect. 3.3.2). The geopotential height at 500 hPa depicts the typical *Omega*-like structure with high geopotential over central Scandinavia, flanked by one pronounced trough upstream over the Northern Atlantic and one downstream over Western Russia (Fig. 4b). Subsequently, the two troughs turned into enclosed cut-off lows filled with relatively cold air and finally merged into one system located over central Europe on 15 May (not shown). In the third week of May, the cut-off moved slowly northeastward on an erratic track while gradually dissipating over central and eastern Europe, leaving a moderately warm and dry air mass with weak gradients over central Europe (Fig. 4c).

The study period from 22 May to 12 June was characterized by a rather stationary and persistent synoptic situation with a pronounced blocking ridge stretching from Iceland over the North Sea to Scandinavia and Northeast Europe (Fig. 5a). As a consequence of the synoptic setting during this episode, the mid-tropospheric flow was weak over most parts of Europe (see Sect. 3.3.3). On average, the ridge was flanked by long-wave troughs: one on the western side with the axis pointing from Baffin Bay to Newfoundland, the other on the eastern side stretching from the Barents Sea to Kazakhstan, while the ridge remained relatively stationary centered over the North Sea region (Fig. 4c-f).

A noticeable feature in the mean 500 hPa geopotential height for this episode (Fig. 5a) is a locally enclosed geopotential minimum over the Bay of Biscay and its surroundings that emerges from repeating/transient cut-off lows forming on the upstream side of the blocking ridge. On 25 May (Fig. 4d), a cut-off low (C1a) approached Iberia – which merged in the next days with the cut-off located over the Celtic Sea (C1b) – and triggered several storms, first in France and then in Benelux and Germany (cf. Fig. 2). In the following days, a new cut off (C2) formed west of Spain, which subsequently influenced the weather there and disappeared relatively quickly. On 1 June, another cut-off (C3) advanced from the Atlantic (Fig. 4e), with some impact on convective activity over France, and then developed into a shallow low-pressure zone in central Europe. Several convergence lines were formed in that zone. In addition, this situation provided very moist air (vertically integrated water vapor, IWV, well above 30 kg m^{-2} over large areas) until 9 June in eastern France and central Europe (Fig. 4e,f). In the end phase of the study period, the next cut-off low (C5) with its associated fronts and convergence lines affected the western half of France and central and southern Germany and lasted until 12 June (Fig. 4f). Simultaneously, a cut-off (C6) over the British Isles influenced the weather in northern Europe.

The geopotential anomalies at the 500 hPa level, calculated as the deviation from the climatological mean (1981 – 2010), exhibit for the study period significant positive values of up to 200 gpm west of Norway (Fig. 5). In contrast, the area over southwestern Europe is reflected by negative geopotential anomalies of more than 50 gpm. Qualitatively similar anomaly patterns are seen in the sea-level pressure distribution (not shown). Simultaneously, the IWV (Fig. 5b) showed distinct positive anomalies of up to 9 kg m^{-2} with a 22-day average of 24 – 28 kg m^{-2}. This finding is in line with the sequential progression of several cut-off lows approaching southwestern Europe and leading to repeating the advection of warm and moist air masses towards central and western Europe during the study period.

3.3.2 North Atlantic-European Weather Regimes

In terms of the North Atlantic-European weather regimes, the large-scale flow situation in May was dominated by simultaneously active life cycles of a Zonal regime (ZO; red in Fig. 6) and European Blocking (EuBL; green). Climatologically, the Zonal regime is characterized by a negative 500 hPa geopotential height anomaly centered over southern Greenland and Iceland, accompanied by a weak positive anomaly over central Europe. The climatological European Blocking regime is characterized by a strong positive geopotential height anomaly over the North Sea region, and a weak negative anomaly over Baffin Bay.

The strong projection in both regimes in May suggests that both the cyclonic anomaly in the Icelandic region and the positive anticyclonic anomaly over Europe were pronounced but altered in their intensities – as discussed in the previous section. The alternating dominance of either regime in the first three weeks of May (Fig. 6) reflects the change of zonal to meridional circulation and the persistent blocking situation during our study period. It is striking that enhanced convection and thunderstorm activity over Europe co-occurred with a weakening of the projection in the Zonal regime (cf. Sect. 3.1). Specifically the first period of widespread thunderstorms (9 – 16 May; cf. Fig. 2) coincides with a weakening of zonal conditions and a dominance of European Blocking from 11 to 18 May. This is interrupted by more zonal conditions from 19 to 21 May, leading to a substantial weakening of convective activity. The convectively most active period from 26 May to 1 June co-occurs with a very strong projection into European Blocking and ends when the blocking decays. On 3 June, a transition into the Atlantic Ridge regime occurs, with blocking shifting into the Northeast Atlantic and western Europe, which coincides with the last episode of an increased number of convective events from 6 to 12 June.

3.3.3 Local-scale environmental conditions

During the entire May/June period, atmospheric stability was very low over large parts of the study domain as indicated by sounding data (Fig. 7a). The SLI values reached negative values almost every day at 12 UTC at one sounding station at least. During the first thunderstorm episode from 9 to 16 May with several heavy rain and hail events (cf. Fig. 2), several stations already show negative SLI values at some days. During the study period, all soundings (with a few exceptions) exhibit permanently negative SLI values; most of the time the values are far below the basic/strict criterion TH_{BC}/TH_{SC} of PIP16 (cf. Sect. 2.5). For example, the median of the SLI during the study period was lower than –3.0 K for Stuttgart, Munich, Vienna, Trappes, and Payerne. Such low values represent very conducive conditions for thunderstorm formation (e.g., Haklander and van Delden, 2003; Manzato, 2003; Sánchez et al., 2009; Kunz, 2007; Mohr and Kunz, 2013). In the ECMWF analysis (Fig. 8a), the SLI average over the study period (12 UTC) was negative for most parts of the domain except for northern Germany, where thunderstorms occurred infrequently. Furthermore, over large parts of the study domain, the stricter criterion (TH_{SC}) was also reached. Due to the upcoming westerly flow at the end of the study period, instability decreases significantly and SLI returns to positive values less conducive for deep moist convection (Fig. 7a).

Due to the low-pressure gradient that prevailed during the study period (Fig. 5), horizontal wind speed in the mid-troposphere was likewise exceptionally low. During the first half of May, 500 hPa wind speeds v_{500hPa} were already low in the sounding data with values rarely exceeding 15 m s^{-1} (Fig. 7b), but further dropped significantly at the beginning of the study period. Averaged over the entire study period, median v_{500hPa} was 7 m s^{-1} at the Essen sounding station; at Stuttgart, Munich, and Vienna values were even lower at around 5 m s^{-1}. At the other three stations in France and Switzerland, the median was between 8 and 10 m s^{-1}. The observations are in line with ECMWF analysis, where v_{500hPa} was between 5 and 10 m s^{-1} on average (particularly low in large parts of Germany and Austria; Fig. 8b).

Because of the low wind speed in the mid-troposphere, most of the thunderstorms moved very slowly or even became stationary. According to the cell tracking analysis during the study period (only Germany; Sect. 2.1.5), approximately half of all convective cells reaching a radar reflectivity of at least 55 dBZ (47.3 % from 480 cells) showed a propagation speed of less than 5 m s^{-1}, and only a few convective cells (1.5 %) had a speed above 15 m s^{-1} (Fig. 9). Mean (standard deviation) and median values are 5.9 m s^{-1} ($\pm$ 2.9 m s^{-1}) and 5.2 m s^{-1}, respectively, which is almost half of the long-term values (cf. Sect. 5.1).

4 Thunderstorms related to cut-off lows

As described in the previous section, the blocking situation over central Europe and the North Sea during the study period was accompanied by a negative geopotential height anomaly over the Iberian Peninsula (Fig. 5), which corresponds well with a significantly enhanced frequency of PV cut-offs of more than 50 % in the Bay of Biscay region (Fig. 10). This region of enhanced PV cut-off frequencies expands over vast parts of Spain, western France and some parts of the British Isles with frequencies often above 25 %, but does not reach Germany or eastern Europe. The fact that relatively high PV cut-off frequencies expand over a larger region of western Europe underlines that multiple individual PV cut-offs form on the upstream flank of the blocking ridge, and intermittently move across Iberia, France, the British Isles, the North Sea, and Germany (see Fig. 4).

In such a configuration, filaments of positive PV that separate from the main PV cut-off may favour lifting on their downstream flank and trigger deep moist convection over larger areas. This relation is exemplarily shown for a 2-day period from 31 May to 1 June representing the end of the period with the most lightning activity and ESWD reports. Here, more than 700,000 lightning strikes were measured over the study domain (black bars in Fig. 11) and more than 70 % of these can be attributed to PV cut-off activity (light grey bars). On 31 May, in the early afternoon, thunderstorms primarily affected Belgium and the Netherlands first (Fig. 12a), before lightning activity re-emerged over central and northern France, Switzerland, and various parts of Germany (Fig. 12b). Several of these events were documented by heavy rain reports in the ESWD (cf. Fig. 2). During the following night, the slow-moving multicellular system moved from Switzerland northwards affecting the southwestern and the western parts of Germany (Fig. 12c,d; cf. Sect. 3.2). While the system dissipated in the late morning over the border region of Germany and Belgium, severe thunderstorms developed again over eastern and northern Germany, Czech Republic, western Poland, and the Pyrenees (Spain; Fig. 12e,f). The link to upper-level PV filaments becomes apparent by carefully investigating the 6-hour evolution of the identified cut-off low masks (Fig. 12; cf. Sect. 2.4). Additionally, the area of negative ω values indicates upward vertical motion over larger areas (green). Generally, this point is expected downstream of a trough/PV cut-off due to vertically increasing advection of PV in combination with layer thickness advection and destabilization underneath the high PV air, which is well represented in our example. On 31 May, a narrow trough accompanied by the cut-off low (C3) approached from the Atlantic to Iberia (cf. Fig. 4e). The areas of ascent on 31 May (Fig. 12a) correspond well with the regions of thunderstorm development in southeastern Germany, central France and the Netherlands (Fig. 12b). From 12 UTC until 18 UTC the next day, this trough narrowed while moving gradually northeastward accompanied by enhanced lightning activity moving from Central France and southern Germany to northeastern Germany and Poland (Fig. 12e,f). It is especially apparent that the multicellular system, which developed in the evening hours of 31 May and was already mentioned at the end of Section 3.2, emerged in a region of negative ω values ahead of the trough (Fig. 12c). On 1 June ascent occurs further to the east over Austria, the Czech Republic and northeastern Germany (Fig. 12e), which agrees well with the location of thunderstorm initiation.

The above discussion of PV filament evolution and lightning activity from 31 May to 1 June revealed an apparent link of this feature with lighting activity confined to the downstream side of PV filaments, where lifting is favoured. Considering the entire study period, we found 53 % of the lightning linked to a nearby PV cut-off (Fig. 11). Examining individual days reveals that on the day with the highest number of lightning detections (29 May) over 85 % of these events can be linked to a PV cut-off. Six out of eight days with the highest number of lightning flashes were between 27 May to 1 June. During this period, more than 75 % of the lightning strikes can be connected with one of the PV cut-offs. We conclude that cut-off low activity provided the necessary environment that favoured lifting within the prevailing unstable air mass and thus helped to trigger widespread thunderstorm activity in western and central Europe during this period.

5 Historical context

In this section, we assess the exceptional nature of the thunderstorm event, by relating the observed precipitation totals, the prevailing environmental conditions, and the occurrence of cut-off systems to the long-term data record.

5.1 Return periods of rainfall and propagation speed of convective cells

To estimate the severity of the rainfall with respect to climatology, we computed return periods (RPs) for each day during the study period in the REGNIE long-term record based on Equation (3). Afterward, we determined the highest RP (largest 24-hour rain total) for each grid point. Because long-term (> 50 years), highly-resolved (1 km^2) and area-wide precipitation data are available only for Germany, we restrict our analysis to this area.

Extreme precipitation generally occurred locally, and only a few smaller regions were affected by high rainfall totals exceeding RPs of 5 years (Fig. 13). RPs in excess of 10 years were restricted to the southern parts of Germany (south of 52°N), except for a few grid points south of Berlin. Most of the precipitation fields with higher RPs occurred as clusters; for example, those near the border to France in Rhineland Palatinate and the Saarland (near Saarbruecken), northeast of Stuttgart, around Bad-Elster Sohl, or north of Munich. Several local maxima have RPs of up to 50 years, but a few hot spots, unevenly distributed in southern Germany, reach values in excess of 200 years (e.g., the observation in Bad Elster-Sohl; cf. Sect. 3.2). For those lo-

https://doi.org/10.5194/wcd-2020-1
Preprint. Discussion started: 14 January 2020

cations, of course, precipitation was extreme, partly with new all-year records. Several hot spots have an almost circular shape with the highest value located in the center.

This characteristic likely reflects the very slow propagation of the thunderstorms, which was substantially lower during the study period compared to climatology (Fig. 9). Generally, convective storms detected between 2005 and 2017 (May/June: 3,428 cells) show significantly higher values of $10.2 \pm 4.9\,\mathrm{m\,s^{-1}}$ (mean ± std) and $9.5\,\mathrm{m\,s^{-1}}$ (median) compared to $5.9 \pm 2.9\,\mathrm{m\,s^{-1}}$ and $5.2\,\mathrm{m\,s^{-1}}$ in the study period. Only 14.4 % of all detected cells show values below $5\,\mathrm{m\,s^{-1}}$, which differs significantly from the proportion in the study period with 47.3%. 15.5 % of the events propagated with a speed of at least $15\,\mathrm{m\,s^{-1}}$ (study period only 1.5%; cf. Sect. 3.3.3).

5.2 Environmental conditions

We begin the analysis of the environmental conditions by comparing the SLI and v_{500hPa} values observed at the seven sounding stations during the study period with the annual minimum of 22-day (same duration as study period) running mean values for May and June during a 30-year period (1981 – 2010; Fig. 14). The box-and-whisker plots on the left represent conditions during our study period (all 22 daily values) and on the right the historical situation. The latter is represented by the annual minimum values (in the sum of 30 values) from comparable periods. Recall that the low values for both SLI and v_{500hPa} were the peculiarity during the 2018 thunderstorm episode. Therefore, we are looking for comparably low values in the 30-year comparison period. By doing so, each of the 30 values taken into account in the right box-plot of each station has the same temporal dimension (running mean of a 22-day period) as the median in the left box-plot of each station.

Both for atmospheric stability and mid-tropospheric flow speed, the interquartile range (the middle 50 % of all values) of the left box-plot is mostly lower than the interquartile range of the right box-plot, illustrating the exceptional environmental conditions of the 2018 thunderstorm episode. This applies in particular to the stations in Germany and Austria; stations in France and in Switzerland tend to overlap (slightly) between the two interquartile ranges. As already mentioned in Sect. 3.3.3, a large portion of SLI and v_{500hPa} values during the event (left box-plot) are well below the basic and strict thresholds TH_{BC} and TH_{SC} (cf. Sect. 2.5) indicating persistence of concurrent low SLI and v_{500hPa} values .

To elaborate on both the peculiarity of the co-occurrence of low stability and weak mid-tropospheric flow and the persistence, we investigate the probability of concurrent events (CE) by following the methodology of PIP16 (see Sect. 2.5) using the same criterion TH_{BC}. The cluster lengths of CE for each of the seven sounding stations during the extended study period in 2018 varies between 5 (Trappes) and 28 days (Munich; cf. legend in Fig. 15). At all three German stations, the defined concurrent conditions prevailed over an extraordinarily long period (Essen: 17 days incl. 3 skip days; Stuttgart: 21 days incl. 1 skip days; Munich 28 days incl. 3 skip days).

In order to assess the occurrence probability of CE cluster lengths with long duration, we compare the cluster lengths for the 2018 thunderstorm episode with a frequency analysis of CE between 1981 and 2017 for each sounding station considering the same months (May/June; Fig. 15). In this way, the relative frequency of the cluster length n in Figure 15 is determined by dividing the absolute number of clusters with the length n by the total number of all clusters. For example, the total number of all clusters is approximately 100 for Trappes, Bordeaux, and Essen, approximately 150 for Stuttgart and Payerne, and

https://doi.org/10.5194/wcd-2020-1
Preprint. Discussion started: 14 January 2020

approximately 200 for Munich and Vienna reflecting the climatological distribution (north-to-south and west-to-east gradient) of atmospheric stability (Mohr and Kunz, 2013).

The exceptional nature of the atmospheric conditions in 2018 is supported by the fact that, for example, the maximum cluster length of 19 days between 1981 and 2017 (observed in Vienna) was exceeded in 2018 by two of the considered sounding stations (Stuttgart, Munich). Additionally, when examining the individual stations, it can be seen that the CE cluster lengths of 2018 at the stations Stuttgart, Essen, Munich and Payerne have never been observed since 1981. The same applies to the Stuttgart sounding compared with the results in PIP16, where so far a maximum CE cluster length of 16 days (1960 – 2014, but summer half-year) has been calculated. Furthermore, the relative frequency of CE clusters at the other stations (Trappes, Bordeaux, Vienna) is also rare (0.5 – 2 %).

5.3 Cut-off lows

In May and June, cut-off lows particularly affected southern Europe and the Mediterranean region. The highest frequency during the climatological period from 1981 to 2010 is found over Portugal and Turkey but with values of less than 4 % (contour in Fig. 16; cf. Nieto et al., 2007b; Wernli and Sprenger, 2007). During the 2018 thunderstorm episode, the anomaly of the PV cut-off frequency from the climatological mean was exceptionally large with maximum values of around 40 % confined to northern Iberia and the Bay of Biscay in western Europe. This means, for example, that PV cut-offs were present on approximately 26 of the 61 days during May and June. The region of anomalous PV cut-off activity expands northward over the British Isles and the adjacent Atlantic Ocean and the North Sea, still with an excess of 20 % (around 12 of 61 days). In other regions, PV cut-off occurrence was similar to the climatological mean. We conclude that the unusual blocking situation over Europe effectively caused cut-off formation on its upstream flank, which then supported a (synoptic) lifting mechanism – the third ingredient for thunderstorm development, together with instability and available moisture.

6 Discussion

It is well known that deep moist convection depends on three necessary but not sufficient ingredients (e.g., Johns and Doswell, 1992; Fuelberg and Biggar, 1994; Trapp, 2013): any kind of instability (conditional, latent, potential) over a layer of sufficient depth, sufficient moisture in the lower troposphere, and a lifting mechanism for the triggering of convection. A further relevant condition for the evolution of deep moist convection is the vertical wind shear or, more generally, the wind at mid-tropospheric levels, which is decisive not only for the organizational form, the longevity and thus the severity of the convective storms (e.g., Weisman and Klemp, 1982; Thompson et al., 2007; Dennis and Kumjian, 2017), but also for their propagation (Corfidi, 2003).

In this study, we investigated the synoptic characteristics of an unusual three-week period of thunderstorm activity in central Europe in May/June 2018. Interestingly, atmospheric blocking was key to providing the large-scale setting conducive for convective in its vicinity. Because of the influence of large-scale mechanisms related to the block and affecting the entire continent, a very high number of thunderstorms affected large parts of western and central Europe during an unusually long period of three weeks. At the beginning of the thunderstorm period, southwesterly flow induced the advection of warm and moist air masses into central Europe. Several studies have identified such a flow to provide convection-favouring conditions (e.g., van Delden, 2001; Kapsch et al., 2012; Mohr, 2013; Merino et al., 2014; Wapler and James, 2015; Nisi et al., 2016; Piper et al., 2019; Mohr et al., 2019). Subsequently, the low-pressure gradient associated with the blocking anticyclone over the (adjacent) European sector prevented a significant air mass change. Thus, moist and conditionally unstabe stratified air masses were trapped in a stationary flow on the southern flank of high pressure for more than three weeks. A few authors have already identified atmospheric blocking as a relevant influencer for widespread thunderstorms. PIP16, for example, showed that the exceptional thunderstorm episode in 2016 in Germany was related to the sequence of Scandinavian and European Blocking. Santos and Belo-Pereira (2019) identified a blocking-like dynamical structure in addition to a Western European and a Scandinavian trough to be responsible for approximately three-quarters of all hail events across Portugal. By combining ERA-Interim reanalysis and lightning detections over a 14-years period, Mohr et al. (2019) found that the presence of a block over the Baltic Sea is frequently associated with increased odds of thunderstorm occurrence due to convection-favouring conditions on its western flank (southwesterly advection of warm, moist and unstable air masses).

In our investigated case, thunderstorms were often triggered by large-scale lifting associated with upper-level cut-off lows or filaments of high PV that separate from the main PV cut-off. On several days during the peak thunderstorm activity, we found that the majority of thunderstorms (based on lightning detections) can be related to a PV cut-off that favours lifting on its downstream flank. The large positive anomaly in PV cut-off frequency, which seems to be relevant for the exceptionally high number of thunderstorms during the study period, in turn was also related to atmospheric blocking. The latter repeatedly lead to the elongation of troughs on its upstream flanks, which finally led to several cut-off lows. The general flow patterns consisting of this spatially extended ridge flanked by troughs persisted over a period of three weeks. Finally, the stagnant flow at mid-tropospheric levels and thus the low vertical wind shear as a consequence of the blocking (cf. PIP16; Mohr et al., 2019) frequently prevented most thunderstorms from developing into organized systems such as large mesoscale convective systems or supercells (cf. Weisman and Klemp, 1982; Doswell and Evans, 2003; Markowski and Richardson, 2010). Most of the thunderstorms formed as local-scale and short-lived single cells, sometimes re-organized into slow-moving multicellular clusters. Due to the low propagation speed, several thunderstorms were able to produce torrential amounts of rain. These, however, affected only very limited areas.

7 Summary and Conclusions

In our study, we investigated an exceptionally large number of thunderstorms in western and central Europe over a three-week period, mid-May to mid-June 2018, using a combination of observational data and model data to gain a more holistic view of the prevailing dynamical and thermodynamical conditions and the decisive trigger mechanisms for this unusual thunderstorm episode. Additional data over a climatological period helped to place the event in its historical context. The 2018 thunderstorm episode was exceptional due to several reasons: (i) the unusual large number of several thousand thunderstorms that caused more than 5 million lightning strikes (all types) in the study area; (ii) the combination of low stability (negative Lifted Index) and low wind speed at mid-tropospheric levels ($\leqslant 5\,\mathrm{m\,s^{-1}}$ at some locations) that prevailed almost every day during the 22-day

https://doi.org/10.5194/wcd-2020-1
Preprint. Discussion started: 14 January 2020

period; (iii) the large cut-off low frequency that was responsible for the majority of convection triggering; and (iv) the high rainfall totals with several new records (e.g., Dietenhofen 86 mm / 1 h) mainly as a consequence of the low propagation speed of the storms leading to several pluvial flash floods.

The other main conclusions drawn from our analyses are:

- Atmospheric blocking, albeit frequently associated with heatwaves and droughts, provided large-scale environmental conditions favouring convection in its vicinity when unstably stratified air masses are advected and/or become entrapped in stagnant flow.
- In the present paper, blocking is accompanied by a high cut-off frequency on its upstream side, which together with filaments of high PV serve as trigger mechanisms for deep moist convection. Compared to climatology, the number of cut-off lows in parts of the study area during the study period was up to 10 times higher.
- The exceptional persistence of low stability combined with weak wind speed in the mid-troposphere prevailing over more than three weeks in some regions, especially in Germany and Austria, has never been observed during the past climatological period of 30 years. This situation was similar to the 2016 thunderstorm episode documented by PIP16, but with a much longer persistence.
- Blocking often associated with low mid-tropospheric wind speeds/low wind shear (cf. Mohr et al., 2019) reduces the development in severe organized convective systems. However, because of the low propagation speed of the storms related to the low-pressure gradient within the block, torrential rainfalls can occur on a local scale.

A growing understanding of the relationship between atmospheric blocking and deep moist convection can enhance – due to the associated persistence – the forecast horizon of thunderstorms on sub-seasonal time scales beyond the classical weather forecast time scale of a few days. This may, for example, help with disaster management, large outdoor activities, and the agriculture sector. It is only helpful, however, if blocked areas are correctly predicted. Recent studies show that this remains a challenge for present (global/regional) numerical weather prediction and climate models (Ferranti et al., 2015; Grams et al., 2018), which, for example, underestimate the blocking frequency in the Atlantic-European sector (Quinting and Vitart, 2019; Attinger et al., 2019).

In future, we intend to investigate statistically some of this study's results, such as the relationship between blocking, cut-off lows and thunderstorm probability. Furthermore, we want to distinguish between different hazard types (hail, heavy rain, gusts) and associated types of thunderstorms and blocking regimes that reveal possible differences in atmospheric processes (e.g., jet stream).

Acknowledgements. The authors thank the various national weather service (DWD; MeteoSwiss; Météo-France; Royal Netherlands Meteorological Institute, KNMI; Zentralanstalt für Meteorologie und Geodynamik; ZAMG), the European Climate Assessment and Dataset (ECA&D) project, the Blitz-Informationsdienst von Siemens (BLIDS; namely Stephan Thern), the Integrated Global Radiosonde Archive

(IGRA) and the European Severe Storms Laboratory (ESSL) for providing different observational data sets. In addition, we thank the European Centre for Medium-Range Weather Forecasts (ECMWF) for providing the operational analysis and the ERA-Interim reanalysis data. Furthermore, we thank Michael Sprenger (ETH Zurich) for compiling the ERA-Interim PV cutoff climatology and Florian Ehmele (KIT) for the post-processing of the REGINE data (return periods). The contributions of CMG and JWA were funded by the Helmholtz Association as part of the Young Investigator Group „Sub-Seasonal Predictability: Understanding the Role of Diabatic Outflow“ (SPREADOUT; grant VH-NG-1243).

Data availability. REGNIE (doi:10.1127/0941-2948/2013/0436), German precipitation data, and 3D radar data used in this paper are freely available for research and can be requested at DWD. Tracks of severe convective storms were calculated from the DWD radar data and are not freely available, but can be made available on request to Michael Kunz for research. Data from ECA&D can be downloaded via the project website (https://www.ecad.eu), from Météo-France via https://donneespubliques.meteofrance.fr/?fond=rubrique&id_rubrique=26, from MeteoSwiss via https://www.meteoswiss.admin.ch/home/services-and-publications/beratung-und-service/datenportal-fuer-lehre-und-forschung.html, and from ZMAG via https://www.zamg.ac.at/cms/de/klima/produkte-und-services/daten-und-statistiken/messdaten. Sounding data are available from the Integrated Global Radiosonde Archive (https://www.ncdc.noaa.gov/data-access/weather-balloon/integrated-global-radiosonde-archive) and data from the ESWD can be obtained via https://www.eswd.eu (see terms and conditions for academic or commercial use). Lightning data are not freely available, but can be requested from the Blitz-Informationsdienst von Siemens (http://blids.de). ECMWF ERA-Interim reanalysis and operational analysis are also online available via https://apps.ecmwf.int/datasets/data/interim-full-daily and the TIGGE webpage (control forecast step 0; https://apps.ecmwf.int/datasets/data/tigge). The methods to detect cut-off lows based on these data are given in Wernli and Sprenger (2007) and Sprenger et al. (2017) and for weather regimes in Grams et al. (2017).

Author contributions. All KIT authors jointly conceived the research questions of the study, continuously discussed the results and wrote the text passages for their respective contribution. SM analysed the ESWD data and together with JaWi the environmental conditions during the thunderstorm episode and in a historical context. In addition, SM wrote the introduction part together with CMG and the discussion/summary part of the paper together with MK and prepared the final draft version of the paper. JaWi also described the synoptic overview and the rainfall statistics in 2018, which were produced by HJP. The return periods of rainfall were investigated by MK, who also examined the lightning data. MS contributed with the analyses of the storm track data (propagation speed of convective cells). RP generated the PV cut-off data and its relationship to lightning activity was analysed by JaWa and CMG. In addition, CMG contributed with the analysis of the weather regimes. Finally, RP, CMG, and JaWi edited the final draft and provided substantial comments and constructive suggestions for scientific clarification and further improvements.

Competing interests. The authors declare that they have no conflict of interest.

https://doi.org/10.5194/wcd-2020-1
Preprint. Discussion started: 14 January 2020

References

Allen, J. T. and Karoly, D. J.: A climatology of Australian severe thunderstorm environments 1979–2011: Inter-annual variability and ENSO influence, Int. J. Climatol., 34, 81–97, https://doi.org/10.1002/joc.3667, 2014.

Allen, J. T., Tippett, M. K., and Sobel, A. H.: Influence of the El Niño/Southern Oscillation on tornado and hail frequency in the United States, Nat. Geosci., 8, 278–283, https://doi.org/10.1038/ngeo2385, 2015.

Attinger, R., Keller, J. H., Köhler, M., Riboldi, J., and Grams, C. M.: Representation of atmospheric blocking in the new global non-hydrostatic weather prediction model ICON, Meteorol. Z., 28, 429–446, https://doi.org/10.1127/metz/2019/0967, 2019.

Banacos, P. C. and Schultz, D. M.: The use of moisture flux convergence in forecasting convective initiation: Historical and operational perspectives, Weather Forecast., 20, 351–366, https://doi.org/10.1175/WAF858.1, 2005.

Barrett, B. S. and Gensini, V. A.: Variability of central United States April–May tornado day likelihood by phase of the Madden-Julian Oscillation, Geophys. Res. Lett., 40, 2790–2795, https://doi.org/10.1002/grl.50522, 2013.

Barriopedro, D., García-Herrera, R., Lupo, A. R., and Hernández, E.: A climatology of Northern Hemisphere blocking, J. Climate, 19, 1042–1063, https://doi.org/10.1175/JCLI3678.1, 2006.

Barthlott, C., Schipper, J. W., Kalthoff, N., Adler, B., Kottmeier, C., Blyth, A., and Mobbs, S.: Model representation of boundary-layer convergence triggering deep convection over complex terrain: A case study from COPS, Atmos. Res., 95, 172–185, https://doi.org/10.1016/j.atmosres.2009.09.010, 2010.

Beniston, M., Stephenson, D. B., Christensen, O. B., Ferro, C. A. T., Frei, C., Goyette, S., Halsnaes, K., Holt, T., Jylhä, K., Koffi, B., Palutikof, J., Schöll, R., Semmler, T., and Woth, K.: Future extreme events in European climate: an exploration of regional climate model projections, Clim. Change, 81, 71–95, https://doi.org/10.1007/s10584-006-9226-z, 2007.

Bieli, M., Pfahl, S., and Wernli, H.: A Lagrangian investigation of hot and cold temperature extremes in Europe, Q. J. R. Meteorol. Soc., 141, 98–108, https://doi.org/10.1002/qj.2339, 2015.

Corfidi, S. F.: Cold pools and MCS propagation: Forecasting the motion of downwind-developing MCSs, Weather Forecast., 18, 997–1017, https://doi.org/10.1175/1520-0434(2003)018<0997:CPAMPF>2.0.CO;2, 2003.

Dee, D. P., Uppala, S. M., Simmons, A. J., Berrisford, P., Poli, P., Kobayashi, S., Andrae, U., Balmaseda, M. A., Balsamo, G., Bauer, P., Bechtold, P., Beljaars, A. C. M., Van De Berg, L., Bidlot, J., Bormann, N., Delsol, C., Dragani, R., Fuentes, M., Geer, A. J., Haimberger, L., Healy, S. B., Hersbach, H., Hólm, E. V., Isaksen, L., Kållberg, P., Köhler, M., Matricardi, M., Mcnally, A. P., Monge-Sanz, B. M., Morcrette, J. J., Park, B. K., Peubey, C., De Rosnay, P., Tavolato, C., Thépaut, J. N., and Vitartv, F.: The ERA-Interim reanalysis: Configuration and performance of the data assimilation system, Q. J. R. Meteorol. Soc., 137, 553–597, https://doi.org/10.1002/qj.828, 2011.

Dennis, E. J. and Kumjian, M. R.: The impact of vertical wind shear on hail growth in simulated supercells, J. Atmos. Sci., 74, 641–663, https://doi.org/10.1175/JAS-D-16-0066.1, 2017.

Dole, R. M. and Gordon, N. D.: Persistent anomalies of the extratropical Northern Hemisphere wintertime circulation: Geographical distribution and regional persistence characteristics, Mon. Weather Rev., 111, 1567–1586, https://doi.org/10.1175/1520-0493(1983)111<1567:PAOTEN>2.0.CO;2, 1983.

Doswell, C. A.: The distinction between large-scale and mesoscale contribution to severe convection: A case study example, Weather Forecast., 2, 3–16, https://doi.org/10.1175/1520-0434(1987)002<0003:TDBLSA>2.0.CO;2, 1987.

Doswell, C. A. and Evans, J. S.: Proximity sounding analysis for derechos and supercells: An assessment of similarities and differences, Atmos. Res., 67, 117–133, https://doi.org/10.1016/S0169-8095(03)00047-4, 2003.

https://doi.org/10.5194/wcd-2020-1
Preprint. Discussion started: 14 January 2020

Dotzek, N., Groenemeijer, P., Feuerstein, B., and Holzer, A. M.: Overview of ESSL's severe convective storms research using the European Severe Weather Database ESWD, Atmos. Res., 93, 575–586, https://doi.org/10.1016/j.atmosres.2008.10.020, 2009.

Drüe, C., Hauf, T., Finke, U., Keyn, S., and Kreyer, O.: Comparison of a SAFIR lightning detection network in northern Germany to the operational BLIDS network, J. Geophys. Res. Atmos., 112, D18 114, https://doi.org/10.1029/2006JD007680, 2007.

Durre, I., Vose, R. S., and Wuertz, D. B.: Overview of the integrated global radiosonde archive, J. Climate, 1151, 53–68, https://doi.org/10.1175/JCLI3594.1, 2006.

DWD: REGNIE: Regionalisierte Niederschläge Verfahrensbeschreibung und Nutzeranleitung, Deutscher Wetterdienst (DWD), Abteilung Hydrometeorologie, Offenbach, Germany. Available from: https://www.dwd.de/DE/leistungen/regnie/regnie.html?nn=353366 (Accessed 13 December 2019), 2018.

Ehmele, F. and Kunz, M.: Flood-related extreme precipitation in Southwestern Germany: Development of a two-dimensional stochastic precipitation model, Hydrol. Earth Syst. Sci., 23, 1083–1102, https://doi.org/10.5194/hess-23-1083-2019, 2018.

ESSL: ESWD Event reporting criteria, Last revision: May 10, 2014, European Severe Storms Laboratory e.V., Munich, Germany. Available from: https://www.eswd.eu/docs/ESWD_criteria_en.pdf (Accessed 13 December 2019), 2014.

Ferranti, L., Corti, S., and Janousek, M.: Flow-dependent verification of the ECMWF ensemble over the Euro-Atlantic sector, Q. J. R. Meteorol. Soc., 141, 916–924, https://doi.org/10.1002/qj.2411, 2015.

Fuelberg, H. E. and Biggar, D. G.: The preconvective environment of summer thunderstorms over the Florida Panhandle, Weather Forecast., 9, 316–326, https://doi.org/10.1175/1520-0434(1994)009<0316:TPEOST>2.0.CO;2, 1994.

Galway, J. G.: The lifted index as a predictor of latent instability, Bull. Am. Meteorol. Soc., 37, 528–529, https://doi.org/10.1175/1520-0477-37.10.528, 1956.

Giaiotti, D., Nordio, S., and Stel, F.: The climatology of hail in the plain of Friuli Venezia Giulia, Atmos. Res., 67–68, 247–259, https://doi.org/10.1016/S0169-8095(03)00084-X, 2003.

Grams, C. M. and Blumer, S. R.: European high-impact weather caused by the downstream response to the extratropical transition of North Atlantic Hurricane Katia (2011), Geophys. Res. Lett., 42, 8738–8748, https://doi.org/10.1002/2015GL066253, 2015.

Grams, C. M., Binder, H., Pfahl, S., Piaget, N., and Wernli, H.: Atmospheric processes triggering the central European floods in June 2013, Nat. Hazards Earth Syst. Sci., 14, 1691–1702, https://doi.org/10.5194/nhess-14-1691-2014, 2014.

Grams, C. M., Beerli, R., Pfenninger, S., Staffell, I., and Wernli, H.: Balancing Europe's wind-power output through spatial deployment informed by weather regimes, Nat. Clim. Change, 7, 557–562, https://doi.org/10.1038/nclimate3338, 2017.

Grams, C. M., Magnusson, L., and Madonna, E.: An atmospheric dynamics perspective on the amplification and propagation of forecast error in numerical weather prediction models: A case study, Q. J. R. Meteorol. Soc., 144, 2577–2591, https://doi.org/10.1002/qj.3353, 2018.

Groenemeijer, P., Púčik, T., Holzer, A. M., Antonescu, B., Riemann-Campe, K., Schultz, D. M., Kühne, T., Feuerstein, B., Brooks, H. E., Doswell, C. A., Koppert, H.-J., and Sausen, R.: Severe convective storms in Europe: Ten years of research at the European Severe Storms Laboratory, Bull. Am. Meteorol. Soc., 98, 2641–2651, https://doi.org/10.1175/BAMS-D-16-0067.1, 2017.

Haklander, A. J. and van Delden, A.: Thunderstorm predictors and their forecast skill for the Netherlands, Atmos. Res., 67–68, 273–299, https://doi.org/10.1016/S0169-8095(03)00056-5, 2003.

Handwerker, J.: Cell tracking with TRACE3D — A new algorithm, Atmos. Res., 61, 15–34, https://doi.org/10.1016/S0169-8095(01)00100-4, 2002.

Hoskins, B. J., McIntyre, M. E., and Robertson, A. W.: On the use and significance of isentropic potential vorticity maps, Q. J. R. Meteorol. Soc., 111, 877–946, https://doi.org/10.1002/qj.49711147002, 1985.

https://doi.org/10.5194/wcd-2020-1
Preprint. Discussion started: 14 January 2020

Johns, R. H. and Doswell, C. A.: Severe local storms forecasting, Weather Forecast., 7, 588–612, https://doi.org/10.1175/1520-0434(1992)007<0588:SLSF>2.0.CO;2, 1992.

Kapsch, M. L., Kunz, M., Vitolo, R., and Economou, T.: Long-term trends of hail-related weather types in an ensemble of regional climate models using a Bayesian approach, J. Geophys. Res., 117, D15 107, https://doi.org/10.1029/2011JD017185, 2012.

Klein Tank, A. M. G., Wijngaard, J. B., Können, G. P., Böhm, R., Demarée, G., Gocheva, A., Mileta, M., Pashiardis, S., Hejkrlik, L., Kern-Hansen, C., Heino, R., Bessemoulin, P., Müller-Westermeier, G., Tzanakou, M., Szalai, S., Pálsdóttir, T., Fitzgerald, D., Rubin, S., Capaldo, M., Maugeri, M., Leitass, A., Bukantis, A., Aberfeld, R., van Engelen, A. F. V., Forland, E., Mietus, M., Coelho, F., Mares, C., Razuvaev, V., Nieplova, E., Cegnar, T., Antonio López, J. A., Dahlström, B., Moberg, A., Kirchhofer, W., Ceylan, A., Pachaliuk, O., Alexander, L. V., and Petrovic, P.: Daily dataset of 20th-century surface air temperature and precipitation series for the European climate assessment, Int. J. Climatol., 22, 1441–1453, https://doi.org/10.1002/joc.773, 2002.

Kunz, M.: The skill of convective parameters and indices to predict isolated and severe thunderstorms, Nat. Hazards Earth Syst. Sci., 7, 327–342, https://doi.org/10.5194/nhess-7-327-2007, 2007.

Kunz, M., Blahak, U., Handwerker, J., Schmidberger, M., Punge, H. J., Mohr, S., Fluck, E., and Bedka, K. M.: The severe hailstorm in SW Germany on 28 July 2013: Characteristics, impacts, and meteorological conditions, Q. J. R. Meteorol. Soc., 144, 231–250, https://doi.org/10.1002/qj.3197, 2018.

Kunz, M., Wandel, J., Fluck, E., Baumstark, S., Mohr, S., and Schemm, S.: Ambient conditions prevailing during hail events in central Europe, Nat. Hazards Earth Syst. Sci. Discuss., in review, https://doi.org/10.5194/nhess-2019-412, 2020.

Lenggenhager, S. and Martius, O.: Atmospheric blocks modulate the odds of heavy precipitation events in Europe, Clim. Dynam., 53, 4155–4171, https://doi.org/10.1007/s00382-019-04779-0, 2019.

Lenggenhager, S., Croci-Maspoli, M., Brönnimann, S., and Martius, O.: On the dynamical coupling between atmospheric blocks and heavy precipitation events: A discussion of the southern Alpine flood in October 2000, Q. J. R. Meteorol. Soc., 145, 530–545, https://doi.org/10.1002/qj.3449, 2018.

Manzato, A.: A climatology of instability indices derived from Friuli Venezia Giulia soundings, using three different methods, Atmos. Res., 67, 417–454, https://doi.org/10.1016/S0169-8095(03)00058-9, 2003.

Markowski, P. and Richardson, Y.: Mesoscale meteorology in midlatitudes, John Wiley & Sons, Chichester, UK, 2010.

Martius, O., Sodemann, H., Joos, H., Pfahl, S., Winschall, A., Croci-Maspoli, M., Graf, M., Madonna, E., Mueller, B., Schemm, S., Sedlacek, J., Sprenger, M., and Wernli, H.: The role of upper-level dynamics and surface processes for the Pakistan flood of July 2010, Q. J. R. Meteorol. Soc., 139, 1780–1797, https://doi.org/10.1002/qj.2082, 2013.

Merino, A., Wu, X., Gascón, E., Berthet, C., García-Ortega, E., and Dessens, J.: Hailstorms in southwestern France: Incidence and atmospheric characterization, Atmos. Res., 140–141, 61–75, https://doi.org/10.1016/j.atmosres.2014.01.015, 2014.

Michel, C. and Rivière, G.: The link between Rossby wave breakings and weather regime transitions, J. Atmos. Sci., 68, 1730–1748, https://doi.org/10.1175/2011JAS3635.1, 2011.

Michelangeli, P.-A., Vautard, R., and Legras, B.: Weather regimes: Recurrence and quasi stationarity, J. Atmos. Sci., 52, 1237–1256, https://doi.org/10.1175/1520-0469(1995)052<1237:WRRAQS>2.0.CO;2, 1995.

Mohr, S.: Änderung des Gewitter- und Hagelpotentials im Klimawandel, Ph.D. thesis, Wiss. Berichte d. Instituts für Meteorologie und Klimaforschung des Karlsruher Instituts für Technologie, Vol. 58, KIT Scientific Publishing, Karlsruhe, Germany, https://doi.org/10.5445/KSP/1000033828, 2013.

Mohr, S. and Kunz, M.: Recent trends and variabilities of convective parameters relevant for hail events in Germany and Europe, Atmos. Res., 123, 211–228, https://doi.org/10.1016/j.atmosres.2012.05.016, 2013.

Mohr, S., Wandel, J., Lenggenhager, S., and Martius, O.: Relationship between atmospheric blocking and warm season thunderstorms over western and central Europe, Q. J. R. Meteorol. Soc., 145, 3040–3056, https://doi.org/10.1002/qj.3603, 2019.

Munich Re: Natural catastrophe statistics online – the new NatCatSERVICE analysis tool, Munich Re, Munich, Germany. Available from: https://www.munichre.com/en/reinsurance/business/non-life/natcatservice/index.html (Accessed 13 December 2019), 2019.

Nachtnebel, H.-P.: New strategies for flood risk management after the catastrophic flood in 2002 in Europe, in: Third DPRI-IIASA International Symposium on Integrated Disaster Risk Management: Coping with Regional Vulnerability, Full Conference Proceedings; 3-5 July 2003, Kyoto International Conference Hall, Kyoto, Japan, 2003.

Nieto, R., Gimeno, L., Añel, J. A., De la Torre, L., Gallego, D., Barriopedro, D., Gallego, M., Gordillo, A., Redaño, A., and Delgado, G.: Analysis of the precipitation and cloudiness associated with COLs occurrence in the Iberian Peninsula, Meteorol. Atmos. Phys., 96, 103–119, https://doi.org/10.1007/s00703-006-0223-6, 2007a.

Nieto, R., Gimeno, L., De la Torre, L., Ribera, P., Barriopedro, D., García-Herrera, R., Serrano, A., Gordillo, A., Redano, A., and Lorente, J.: Interannual variability of cut-off low systems over the European sector: The role of blocking and the Northern Hemisphere circulation modes, Meteorol. Atmos. Phys., 96, 85–101, https://doi.org/10.1007/s00703-006-0222-7, 2007b.

Nieto, R., Sprenger, M., Wernli, H., Trigo, R. M., and Gimeno, L.: Identification and climatology of cut-off lows near the tropopause, Ann. NY Acad. Sci., 1146, 256–290, https://doi.org/10.1196/annals.1446.016, 2008.

Nisi, L., Martius, O., Hering, A., Kunz, M., and Germann, U.: Spatial and temporal distribution of hailstorms in the Alpine region: A long-term, high resolution, radar-based analysis, Q. J. R. Meteorol. Soc., 142, 1590–1604, https://doi.org/10.1002/qj.2771, 2016.

Orlanski, I.: A rational subdivision of scales for atmospheric processes, Bull. Am. Meteorol. Soc., 56, 527–530, 1975.

Pfahl, S. and Wernli, H.: Quantifying the relevance of atmospheric blocking for co-located temperature extremes in the Northern Hemisphere on (sub-)daily time scales, Geophys. Res. Lett., 39, L12 807, https://doi.org/10.1029/2012GL052261, 2012.

Piaget, N., Froidevaux, P., Giannakaki, P., Gierth, F., Martius, O., Riemer, M., Wolf, G., and Grams, C. M.: Dynamics of a local Alpine flooding event in October 2011: Moisture source and large-scale circulation, Q. J. R. Meteorol. Soc., 141, 1922–1937, https://doi.org/10.1002/qj.2496, 2015.

Piper, D. and Kunz, M.: Spatiotemporal variability of lightning activity in Europe and the relation to the North Atlantic Oscillation teleconnection pattern, Nat. Hazards Earth Syst. Sci., 17, 1319–1336, https://doi.org/10.5194/nhess-17-1319-2017, 2017.

Piper, D., Kunz, M., Ehmele, F., Mohr, S., Mühr, B., Kron, A., and Daniell, J.: Exceptional sequence of severe thunderstorms and related flash floods in May and June 2016 in Germany. Part I: Meteorological background, Nat. Hazards Earth Syst. Sci., 16, 2835–2850, https://doi.org/10.5194/nhess-16-2835-2016, 2016.

Piper, D. A., Kunz, M., Allen, J. T., and Mohr, S.: Investigation of the temporal variability of thunderstorms in Central and Western Europe and the relation to large-scale flow and teleconnection patterns, Q. J. R. Meteorol. Soc., 145, 3644–3666, https://doi.org/10.1002/qj.3647, 2019.

Poelman, D. R., Schulz, W., Diendorfer, G., and Bernardi, M.: The European lightning location system EUCLID – Part 2: Observations, Nat. Hazards Earth Syst. Sci., 16, 607–616, https://doi.org/10.5194/nhess-16-607-2016, 2016., 2016.

Portmann, R., Crezee, B., Quinting, J., and Wernli, H.: The complex life cycles of two long-lived potential vorticity cut-offs over Europe, Q. J. R. Meteorol. Soc., 144, 701–719, https://doi.org/10.1002/qj.3239, 2018.

https://doi.org/10.5194/wcd-2020-1
Preprint. Discussion started: 14 January 2020

Puskeiler, M., Kunz, M., and Schmidberger, M.: Hail statistics for Germany derived from single-polarization radar data, Atmos. Res., 178–179, 459–470, https://doi.org/10.1016/j.atmosres.2016.04.014, 2016.

Quinting, J. F. and Vitart, F.: Representation of synoptic-scale Rossby wave packets and blocking in the S2S Prediction Project Database, Geophys. Res. Lett., 46, 1070–1078, https://doi.org/10.1029/2018GL081381, 2019.

Rädler, A. T., Groenemeijer, P., Faust, E., and Sausen, R.: Detecting severe weather trends using an Additive Regressive Convective Hazard Model (AR-CHaMo), J. Appl. Meteorl. Climatol., 57, 569–587, https://doi.org/10.1175/JAMC-D-17-0132.1, 2018.

Rauthe, M., Steiner, H., Riediger, U., A., M., and Gratzki, A.: A Central European precipitation climatology – Part I: Generation and validation of a high-resolution gridded daily data set (HYRAS), Meteorol. Z., 22, 235–256, https://doi.org/10.1127/0941-2948/2013/0436, 2013.

Rex, D. F.: Blocking action in the middle troposphere and its effect upon regional climate: I. An aerological study of blocking action, Tellus, 2, 196–211, https://doi.org/10.3402/tellusa.v2i3.8546, 1950a.

Rex, D. F.: Blocking action in the middle troposphere and its effect upon regional climate: II. The climatology of blocking action, Tellus, 2, 275–301, https://doi.org/10.3402/tellusa.v2i4.8603, 1950b.

Röthlisberger, M. and Martius, O.: Quantifying the local effect of Northern Hemisphere atmospheric blocks on the persistence of summer hot and dry spells, Geophys. Res. Lett., 43, 10 101–10 111, https://doi.org/10.1029/2019GL083745, 2019.

Röthlisberger, M., Martius, O., and Wernli, H.: Northern Hemisphere Rossby wave initiation events on the extratropical jet – A climatological analysis, J. Climate, 31, 743–760, https://doi.org/10.1175/JCLI-D-17-0346.1, 2018.

Sánchez, J. L., Marcos, J. L., Dessens, J., López, L., Bustos, C., and García-Ortega, E.: Assessing sounding-derived parameters as storm predictors in different latitudes, Atmos. Res., 93, 446–456, https://doi.org/10.1016/j.atmosres.2008.11.006, 2009.

Santos, J. A. and Belo-Pereira, M.: A comprehensive analysis of hail events in Portugal: Climatology and consistency with atmospheric circulation, Int. J. Climatol., 39, 188–205, https://doi.org/10.1002/joc.5794, 2019.

Schaller, N., Sillmann, J., Anstey, J., Fischer, E. M., Grams, C. M., and Russo, S.: Influence of blocking on Northern European and Western Russian heatwaves in large climate model ensembles, Environ. Res. Lett., 13, 054 015, https://doi.org/10.1088/1748-9326/aaba55, 2018.

Schemm, S., Nisi, L., Martinov, A., Leuenberger, D., and Martius, O.: On the link between cold fronts and hail in Switzerland, Atmos. Sci. Lett., 17, 315–325, https://doi.org/10.1002/asl.660, 2016.

Schmidberger, M.: Hagelgefährdung und Hagelrisiko in Deutschland basierend auf einer Kombination von Radardaten und Versicherungsdaten, Ph.D. thesis, Wiss. Berichte d. Instituts für Meteorologie und Klimaforschung des Karlsruher Instituts für Technologie, Vol. 78, KIT Scientific Publishing, Karlsruhe, Germany, https://doi.org/10.5445/KSP/1000086012, 2018.

Schröter, K., Kunz, M., Elmer, F., Mühr, B., and Merz, B.: What made the June 2013 flood in Germany an exceptional event? A hydrometeorological evaluation, Hydrol. Earth Syst. Sci., 19, 309–327, https://doi.org/10.5194/hess-19-309-2015, 2015.

Schulz, W., Diendorfer, G., Pedeboy, S., and Poelman, D. R.: The European lightning location system EUCLID – Part 1: Performance analysis and validation, Nat. Hazards Earth Syst. Sci., 16, 595–605, https://doi.org/10.5194/nhess-16-595-2016, 2016.

Soderholm, J. S., McGowan, H., Richter, H., Walsh, K., Weckwerth, T. M., and Coleman, M.: An 18-year climatology of hailstorm trends and related drivers across southeast Queensland, Australia, Q. J. R. Meteorol. Soc., 143, 1123–1135, https://doi.org/10.1002/qj.2995, 2017.

Sousa, P. M., Trigo, R. M., Barriopedro, D., Soares, P. M. M., Ramos, A. M., and Liberato, M. L. R.: Responses of European precipitation distributions and regimes to different blocking locations, Clim. Dynam., 48, 1141–1160, https://doi.org/10.1007/s00382-016-3132-5, 2017.

https://doi.org/10.5194/wcd-2020-1
Preprint. Discussion started: 14 January 2020

Sprenger, M., Fragkoulidis, G., Binder, H., Croci-Maspoli, M., Graf, P., Grams, C. M., Knippertz, P., Madonna, E., Schemm, S., Škerlak, B., and Wernli, H.: Global climatologies of Eulerian and Lagrangian flow features based on ERA-Interim, Bull. Am. Meteorol. Soc., 98, 1739–1748, https://doi.org/10.1175/BAMS-D-15-00299.1, 2017.

Tarabukina, L. D., Antokhina, O. Y., Kononova, N. K., Kozlov, V. I., and Innokentiev, D. E.: Formation of intense thunderstorms in Yakutia in periods of frequent atmospheric blocking in Western Siberia, in: IOP Conf. Ser.: Mater. Sci. Eng., vol. 698, p. 044050, https://doi.org/10.1088/1757-899x/698/4/044050, 2019.

Thompson, R. L., Mead, C. M., and Edwards, R.: Effective storm-relative helicity and bulk shear in supercell thunderstorm environments, Weather Forecast., 22, 102–115, https://doi.org/10.1175/WAF969.1, 2007.

Tibaldi, S. and Molteni, F.: On the operational predictability of blocking, Tellus A, 42, 343–365, https://doi.org/10.1034/j.1600-0870.1990.t01-2-00003.x, 1990.

Trapp, R. J.: Mesoscale-convective processes in the atmosphere, Cambridge University Press, New York, USA, 2013.

van Delden, A.: The synoptic setting of thunderstorms in Western Europe, Atmos. Res., 56, 89–110, https://doi.org/10.1016/S0169-8095(00)00092-2, 2001.

van den Besselaar, E. J. M., Klein Tank, A. M. G., and Buishand, T. A.: Trends in European precipitation extremes over 1951–2010, Int. J. Climatol., 33, 2682–2689, https://doi.org/10.1002/joc.3619, 2013.

Vautard, R.: Multiple weather regimes over the North Atlantic: Analysis of precursors and successors, Mon. Weather Rev., 118, 2056–2081, https://doi.org/10.1175/1520-0493(1990)118<2056:MWROTN>2.0.CO;2, 1990.

Wapler, K.: High-resolution climatology of lightning characteristics within Central Europe, Meteorol. Atmos. Phys., 122, 175–184, https://doi.org/10.1007/s00703-013-0285-1, 2013.

Wapler, K. and James, P.: Thunderstorm occurrence and characteristics in Central Europe under different synoptic conditions, Atmos. Res., 158, 231–244, https://doi.org/10.1016/j.atmosres.2014.07.011, 2015.

Weisman, M. L. and Klemp, J. B.: The dependence of numerically simulated convective storms on vertical wind shear and buoyancy, Mon. Weather Rev., 110, 504–520, https://doi.org/10.1175/1520-0493(1982)110<0504:TDONSC>2.0.CO;2, 1982.

Wernli, H. and Sprenger, M.: Identification and ERA-15 climatology of potential vorticity streamers and cutoffs near the extratropical tropopause, J. Atmos. Sci., 64, 1569–1586, https://doi.org/10.1175/JAS3912.1, 2007.

Wilks, D. S.: Statistical methods in the atmospheric sciences: An introduction – Second Edition, Academie Press, Elsevier, Burlington, USA, 2006.

Wilson, J. W. and Schreiber, W. E.: Initiation of convective storms at radar-observed boundary-layer convergence lines, Mon. Weather Rev., 114, 2516–2536, https://doi.org/10.1175/1520-0493(1986)114<2516:IOCSAR>2.0.CO;2, 1986.

Woollings, T., Barriopedro, D., Methven, J., Son, S.-W., Martius, O., Harvey, B., Sillmann, J., Lupo, A. R., and Seneviratne, S.: Blocking and its response to climate change, Curr. Clim. Change Rep., 4, 287–300, https://doi.org/10.1007/s40641-018-0108-z, 2018.

Wussow, G.: Untere Grenzwerte dichter Regenfälle, Meteorol. Z., 39, 173–178, 1922.

https://doi.org/10.5194/wcd-2020-1
Preprint. Discussion started: 14 January 2020

Table 1. Top list of hourly, 3-hour, and 24-hour rainfall totals within the study domain during the study period (AT = Austria, FR = France, GE = Germany).

Period	Country	Location	Precipitation sum	Time	Coordinates
1 h	GE	Dietenhofen	85.7 mm	31 May 19 h	49.4°N 10.7°E
1 h	GE	Rohr-Dechendorf	71.0 mm	09 June 15 h	49.3°N 10.9°E
1 h	FR	Labécède-Lauragais	64.4 mm	10 June 17 h	43.4°N 2.0°E
1 h	GE	Hohenberg an der Eger	61.4 mm	31 May 18 h	50.1°N 12.2°E
1 h	GE	Lenzkirch-Ruhbühl	59.8 mm	31 May 20 h	47.9°N 8.2°E
1 h	FR	Langres	59.4 mm	05 June 20 h	47.8°N 5.3°E
1 h	FR	Castanet-le-Haut	56.2 mm	30 May 14 h	43.7°N 3.0°E
1 h	GE	Erlbach-Eubabrunn	55.6 mm	31 May 17 h	50.3°N 12.4°E
1 h	FR	Rouvroy-en-Santerre	54.3 mm	28 May 22 h	49.8°N 2.7°E
3 h	FR	Prades-le-Lez	86.8 mm	11 June 12 h	43.7°N 3.9°E
3 h	GE	Bad Elster-Sohl	86.3 mm	24 May 12 h	50.3°N 12.3°E
3 h	AT	Puchberg am Schneeberg	86.3 mm	12 June 12 h	47.8°N 15.9°E
3 h	GE	Dietenhofen	86.2 mm	31 May 18 h	49.4°N 10.7°E
3 h	FR	L'Oudon-Lieury	83.8 mm	28 May 12 h	49.0°N 0.0°E
3 h	FR	Rocroi	79.4 mm	27 May 18 h	49.9°N 4.5°E
3 h	GE	Leutkirch-Herlazhofen	79.1 mm	08 June 15 h	47.8°N 10.0°E
3 h	GE	Kleve	78.8 mm	29 May 15 h	51.8°N 6.1°E
3 h	AT	Sulzberg	78.0 mm	04 June 15 h	47.5°N 9.9°E
24 h	GE	Mauth-Finsterau	166.5 mm	12 June	48.9°N 13.6°E
24 h	GE	Bad Elster-Sohl	154.9 mm	24 May	50.3°N 12.3°E
24 h	GE	Bruchweiler	145.0 mm	27 May	49.8°N 7.2°E
24 h	FR	Monein	130.0 mm	12 June	43.3°N 0.5°W
24 h	FR	Ger	126.4 mm	12 June	43.2°N 0.1°W
24 h	FR	Mont Aigoual (Valleraugue)	124.1 mm	28 May	44.1°N 3.6°E
24 h	FR	Les Bottereaux	123.0 mm	04 June	48.9°N 0.7°E
24 h	FR	Navarrenx	117.0 mm	12 June	43.3°N 0.8°W
24 h	AT	Puchberg am Schneeberg	116.3 mm	12 June	47.8°N 15.9°E

https://doi.org/10.5194/wcd-2020-1
Preprint. Discussion started: 14 January 2020

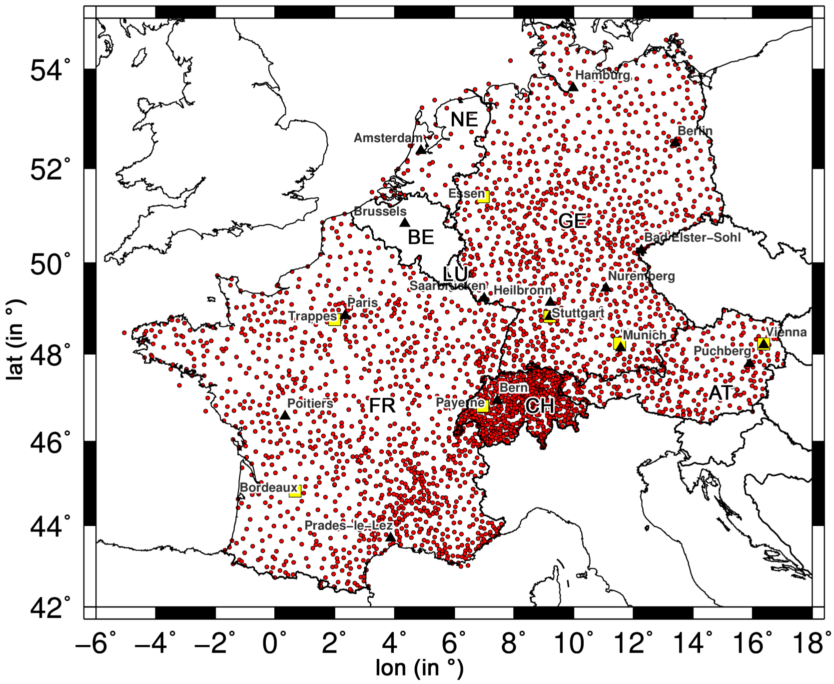

Figure 1. All considered precipitation stations (in red) collected from ECA&D and the three national weather services (France, Germany, Switzerland; see Sect. 2.1.2). In addition, the seven investigated sounding stations are shown (in yellow, see Sect. 2.1.4). Some relevant locations are also presented, which are used in the text. Defined country codes are FR = France, BE = Belgium, NE = Netherlands, LU = Luxembourg (the latter three: Benelux), GE = Germany, CH = Switzerland, AT = Austria.

https://doi.org/10.5194/wcd-2020-1
Preprint. Discussion started: 14 January 2020

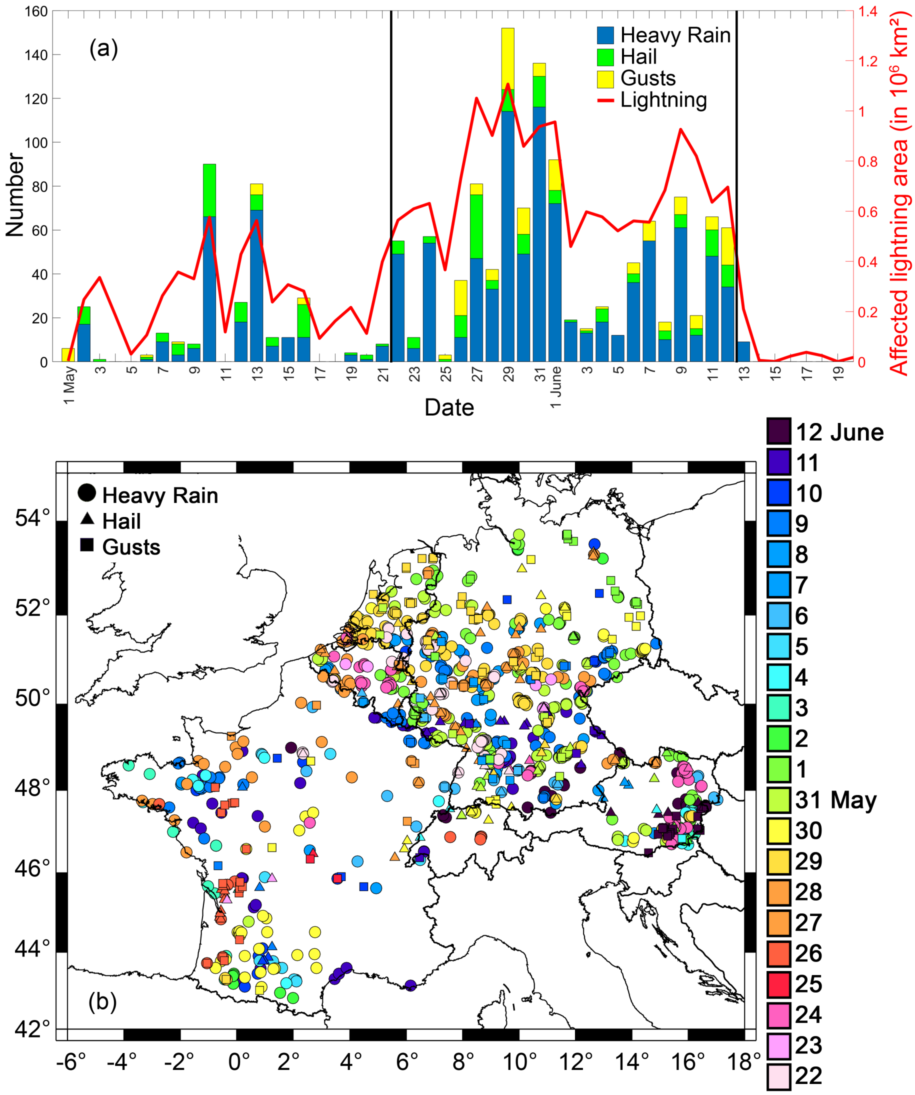

Figure 2. (a) Time series of all recorded ESWD reports (heavy rain in blue, hail in green, convective gusts in yellow) in the study domain during the extended study period including the daily total area affected by lightning in km^2 (in red) and (b) related regional distribution of the different phenomena (heavy rain ●, hail ▲, convective gusts ■) during the study period (22 May to 12 June 2018).

https://doi.org/10.5194/wcd-2020-1
Preprint. Discussion started: 14 January 2020

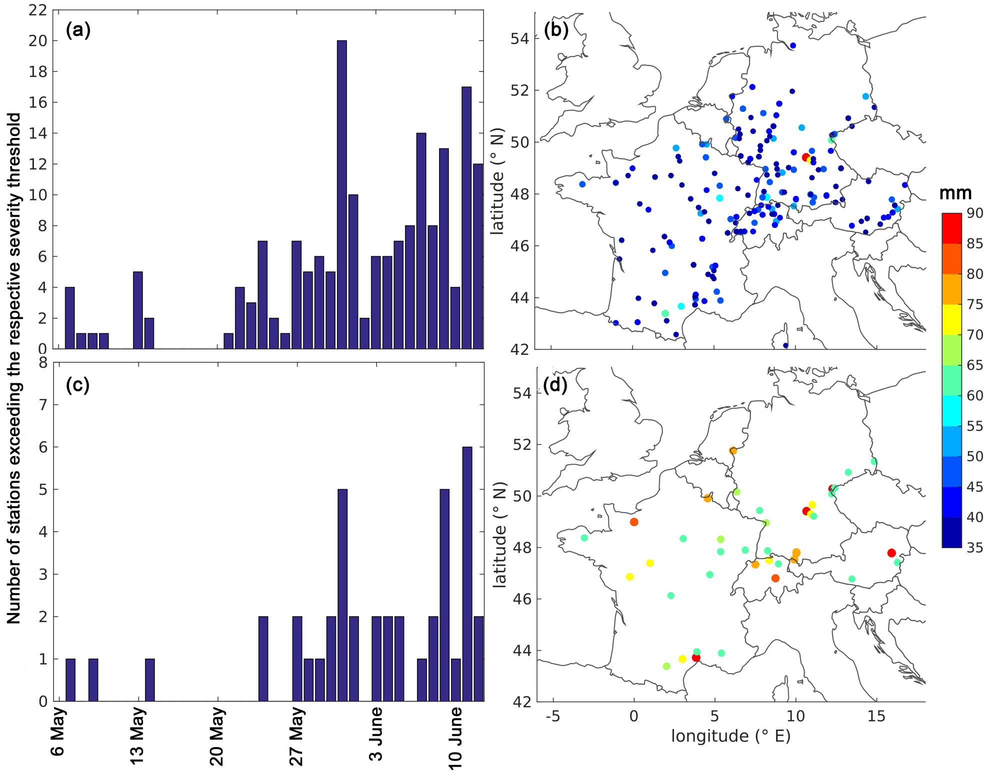

Figure 3. Time series of the number of stations exceeding precipitation thresholds of (a) > 35 mm hourly and (c) > 60 mm over 3-hours including the location and total maximum of (b) hourly and (d) 3-hour sums of the respective station during the study period (22 May to 12 June).

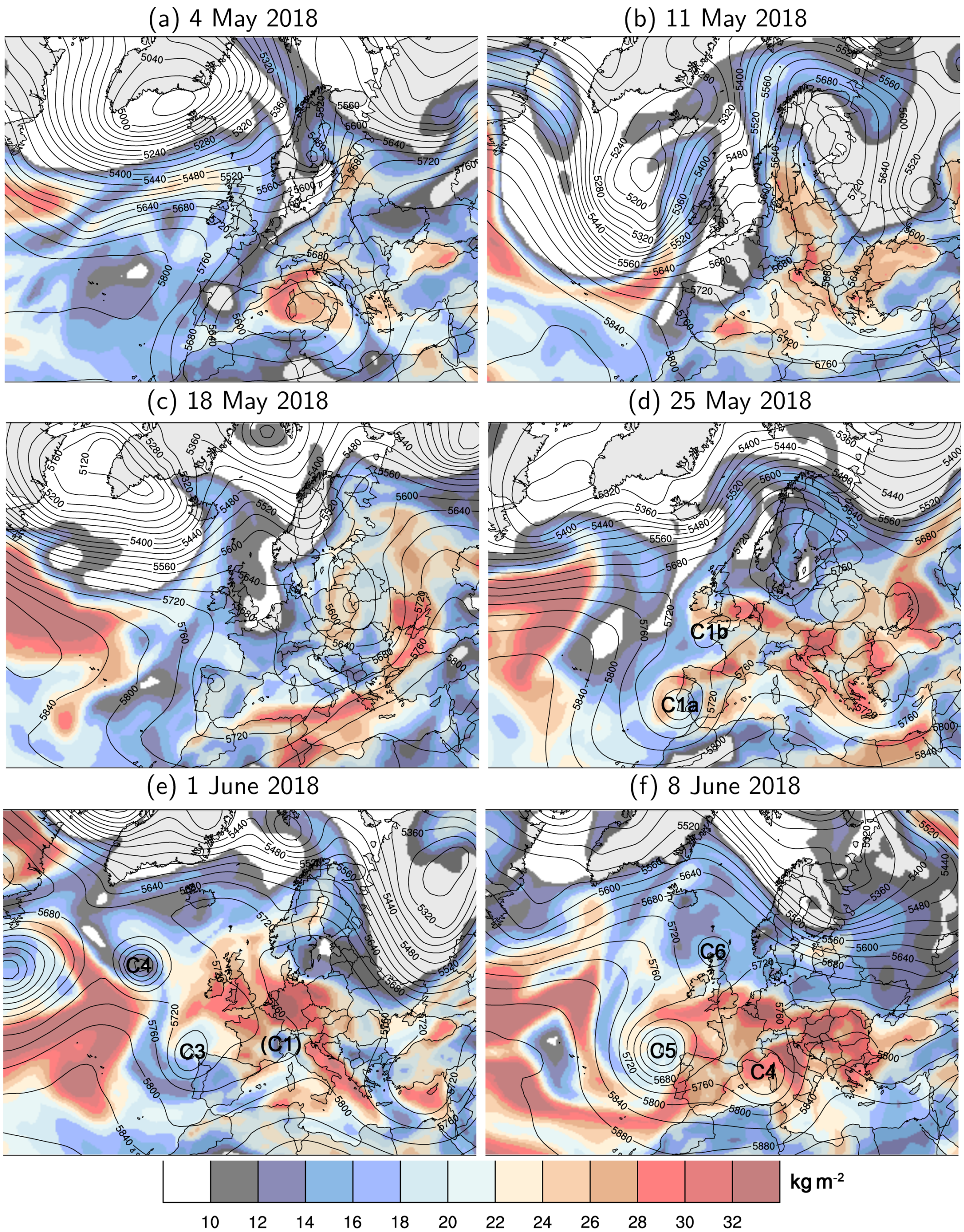

Figure 4. 500 hPa geopotential height (contours every 40 gpm) and vertically integrated water vapor (IWV, shaded in kg m^{-2}) for selected days at 00 UTC during the extended study period: (a) 4 May, (b) 11 May, (c) 18 May, (d) 25 May, (e) 1 June, and (f) 8 June (ERA-Interim). Several cut-off lows during the study period mentioned in the text are indicated with numbers (C1, . . . , C6).

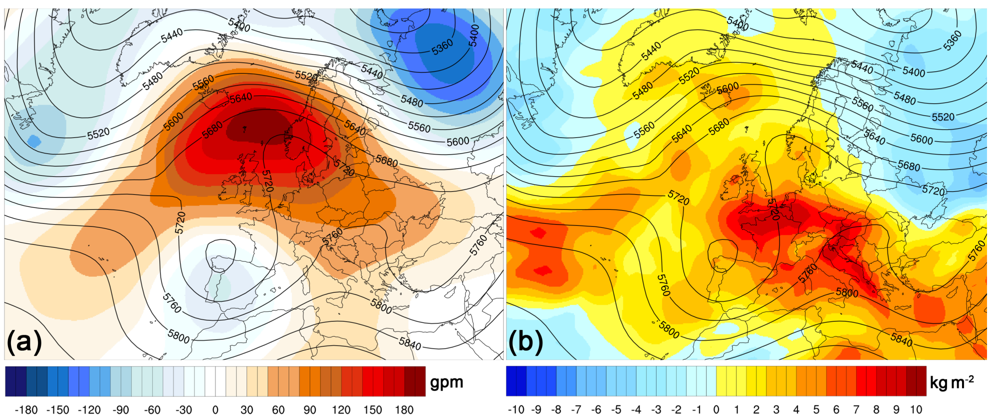

Figure 5. Composite mean 500 hPa geopotential height (contours every 40 gpm) and in (a) anomaly with reference the climatological mean in May and June (1981 – 2010; shaded in gpm) and in (b) together with anomalies of the IWV with reference to the climatological mean in May and June (1981 – 2001; shaded in kg m^{-2} (based on ERA-Interim).

https://doi.org/10.5194/wcd-2020-1
Preprint. Discussion started: 14 January 2020

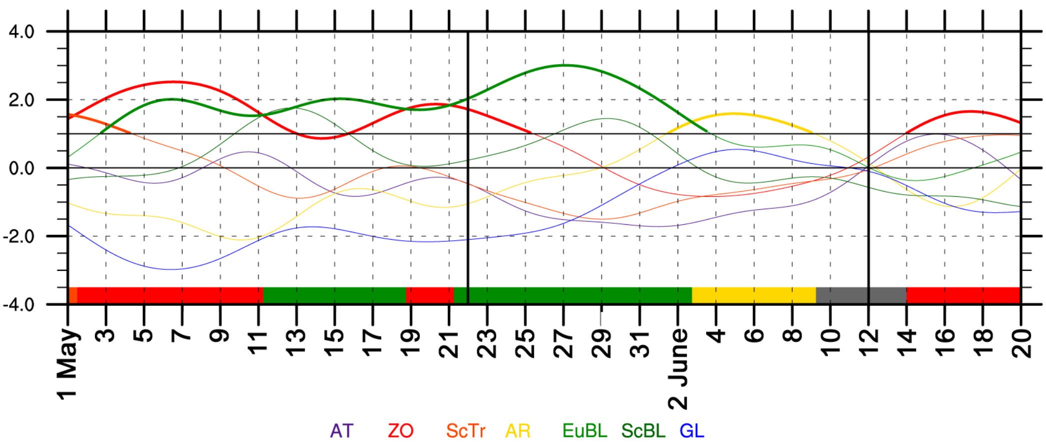

Figure 6. Atlantic-European weather regime life cycles: Normalized projection into all 7 regimes. Active regimes according to the life cycle definition in bold. The bottom colored row shows the active regime with the maximum projection, as Zonal regime (ZO, red), European Blocking (EuBL, green), Atlantic Ridge (AR, yellow), no regime (grey). See text for details (ECMWF analysis).

https://doi.org/10.5194/wcd-2020-1
Preprint. Discussion started: 14 January 2020

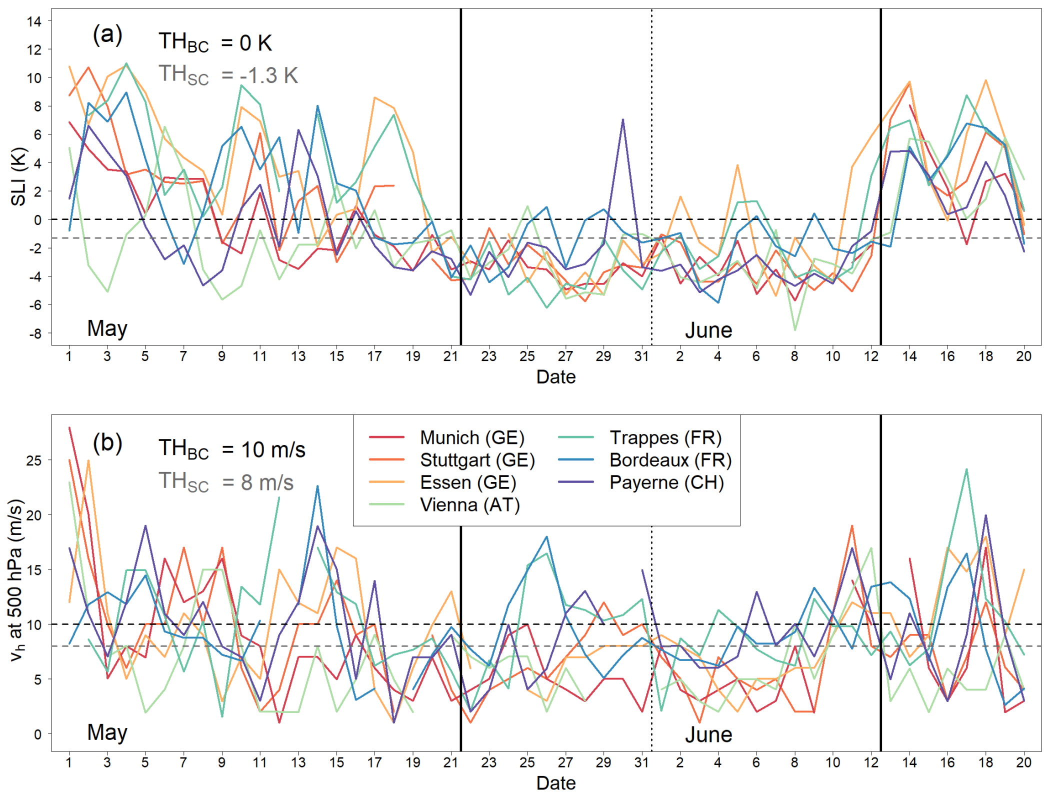

Figure 7. Time series of (a) surface-based Lifted Index (SLI in K) and (b) horizontal wind speed at 500 hPa (in $m\,s^{-1}$) for the 12 UTC sounding at seven central and western European stations in the period 1 May to 20 June 2018. Black and gray dashed lines and numbers indicate thresholds as defined in PIP16 (cf. Sect. 2.5).

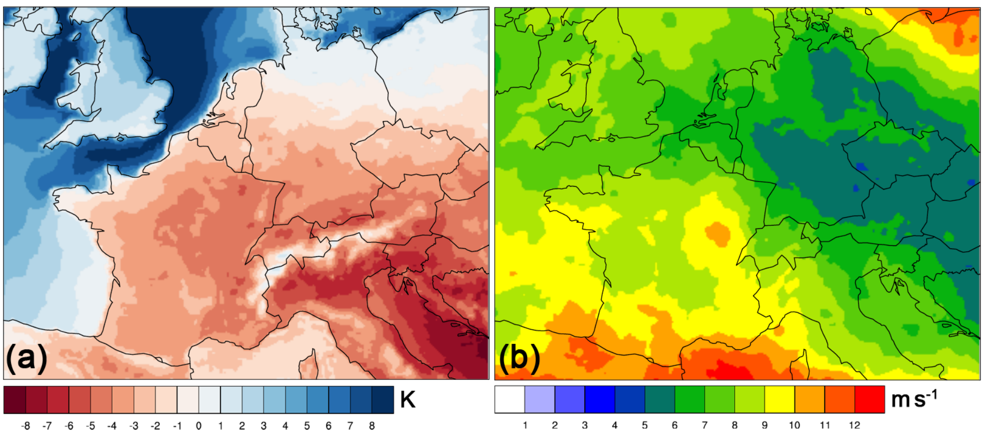

Figure 8. (a) Mean surface-based Lifted Index (SLI in K) and (b) 500 hPa wind speed (in m s^{-1}) for the study period from 22 May to 12 June 2018 based on ECMWF analysis data (both at 12 UTC; ECMWF analysis).

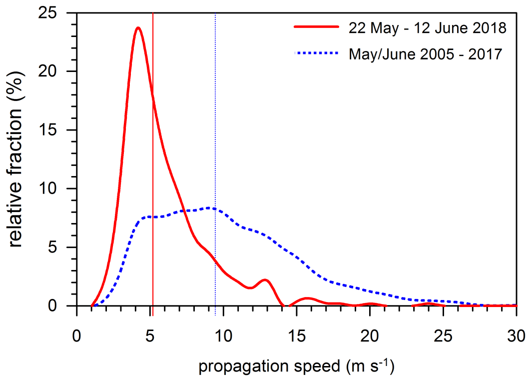

Figure 9. Histogram of the propagation speed of convective cells (increments of 1 m s^{-1}; spline filter) detected by TRACE3D in Germany during the study period (red) and for all convective cells between 2005 and 2017 (May/June; blue); vertical lines indicate the median of the two samples.

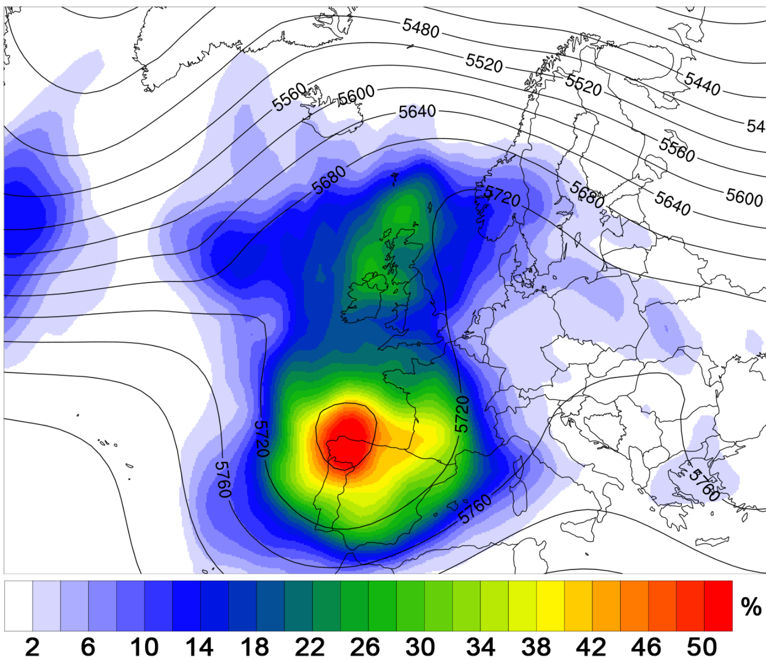

Figure 10. Composite mean of 500 hPa geopotential height (contours every 40 gpm) and cut-off low frequency (color shading in %) during the study period (ERA-Interim).

https://doi.org/10.5194/wcd-2020-1
Preprint. Discussion started: 14 January 2020

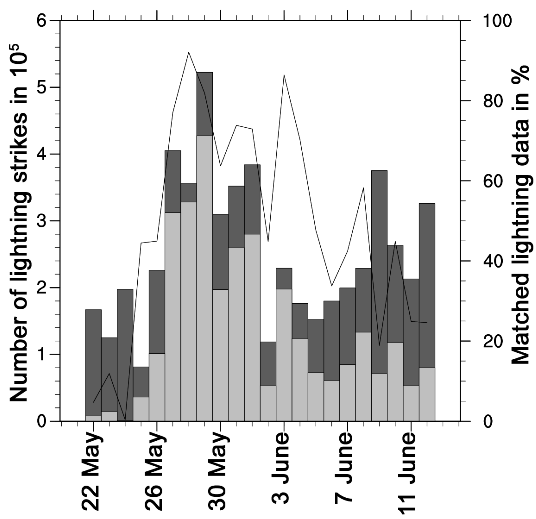

Figure 11. Lightning strikes per day (03 UTC – 03 UTC on the next day) during the study period for all thunderstorm events (dark grey bars) and those thunderstorms that can be linked to a cut-off low (light grey bars). The black line shows the percentage of lightning strikes per day that can be attributed to a cut-off low.

https://doi.org/10.5194/wcd-2020-1
Preprint. Discussion started: 14 January 2020

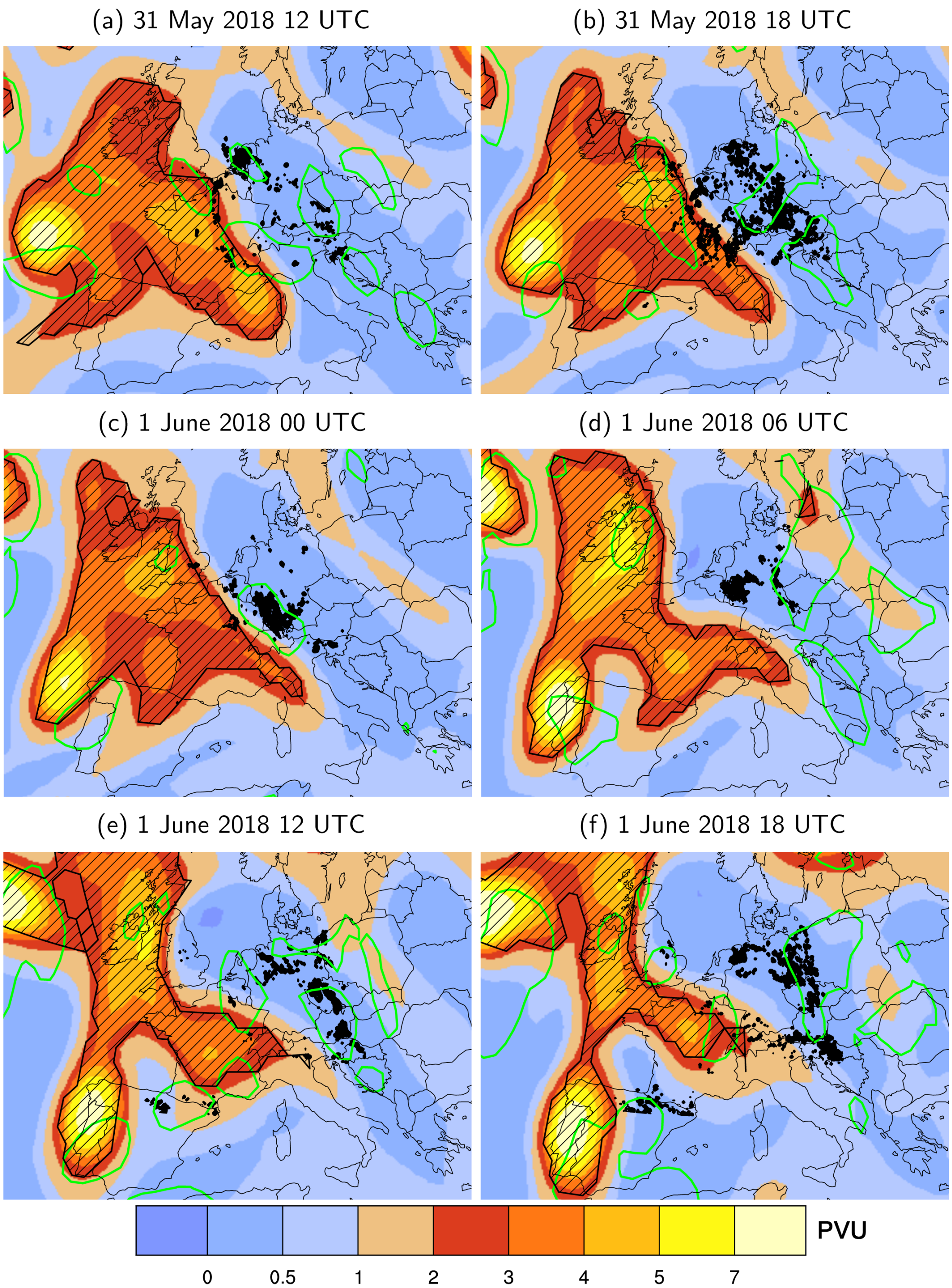

Figure 12. Lightning data (dark black dots) for 6-hour time spans centered around the respective time and PV on the 325 K isentropic surface (shaded in PVU; ERA-Interim). Regions of ascent at 500hPa are indicated by green contours ($\omega = -0.1$ Pa s^{-1}); ERA-Interim). Red hatching indicates masks of objectively identified cut-offs on the 325 K isentropic surface.

https://doi.org/10.5194/wcd-2020-1
Preprint. Discussion started: 14 January 2020

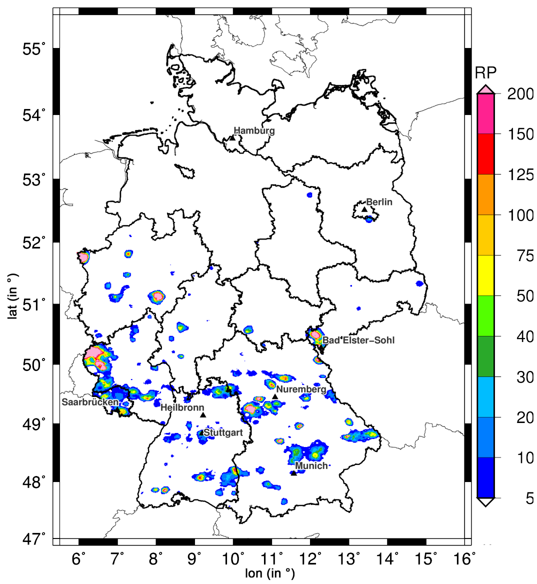

Figure 13. Return periods (RP) of the highest 24-hour precipitation totals that occurred during the study period at each grid point (REGNIE precipitation data; reference period: 1951 – 2017, summer half-year).

https://doi.org/10.5194/wcd-2020-1
Preprint. Discussion started: 14 January 2020

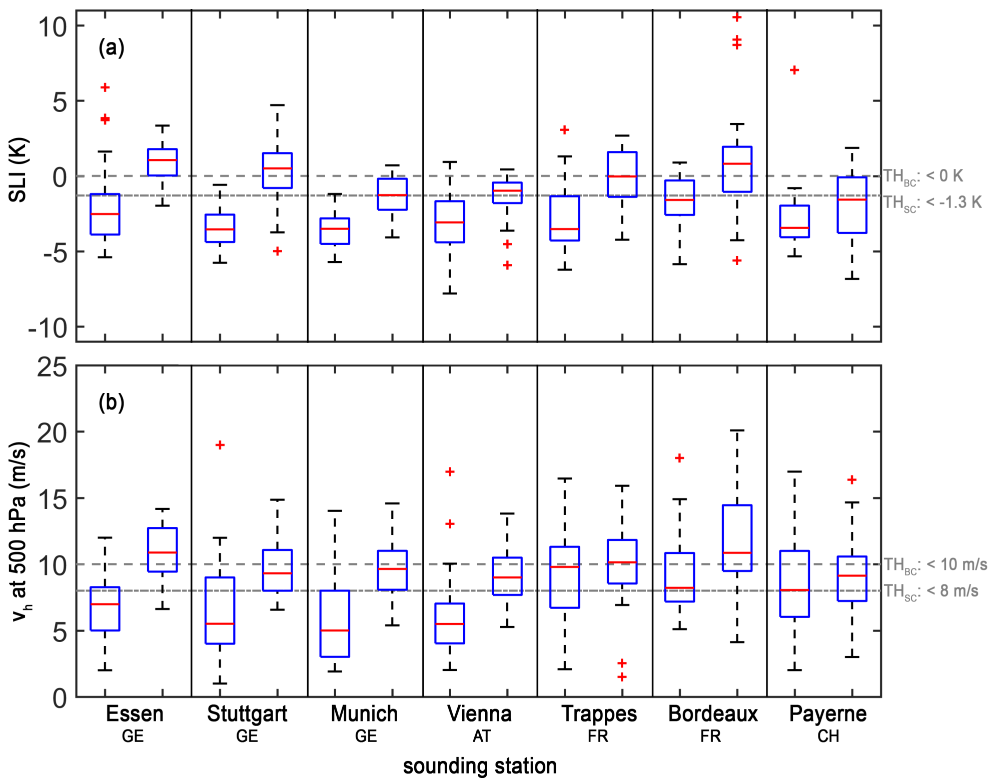

Figure 14. Box-and-whisker plots (median, 1st/3rd quartiles, whisker = +/–2.7σ, outliers) for the seven sounding stations. The left box-plots of each station include all values of (a) SLI and (b) v_{500hPa} during the study period at 12 UTC, the right box-plots include the annual minimum of the running mean (22 days) during May and June between 1981 and 2010. The two gray lines indicate the defined thresholds TH_{BC} and TH_{SC} of PIP16.

https://doi.org/10.5194/wcd-2020-1
Preprint. Discussion started: 14 January 2020

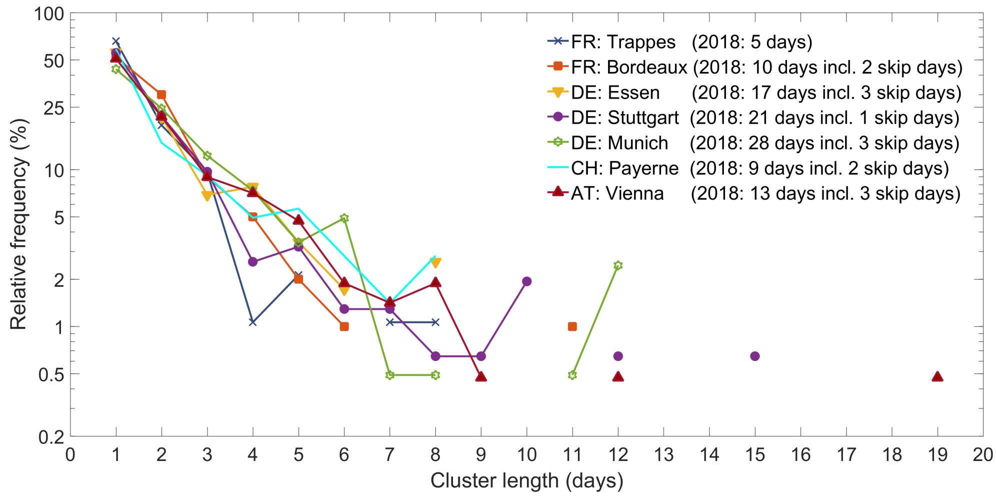

Figure 15. Relative frequency of clusters of consecutive days exceeding the threshold TH_{BC} for concurrent events with low stability ($SLI < 0\,K$) and weak flow $v_{500hPa} < 10\,m\,s^{-1}$) at the seven sounding stations (Trappes, Bordeaux, Essen, Stuttgart, Munich, Payerne, Vienna) during 1981 – 2017 (May/June). Maximum cluster lengths during the extended study period in 2018 (Mai/June) are shown in the legend (including skip days).

https://doi.org/10.5194/wcd-2020-1
Preprint. Discussion started: 14 January 2020

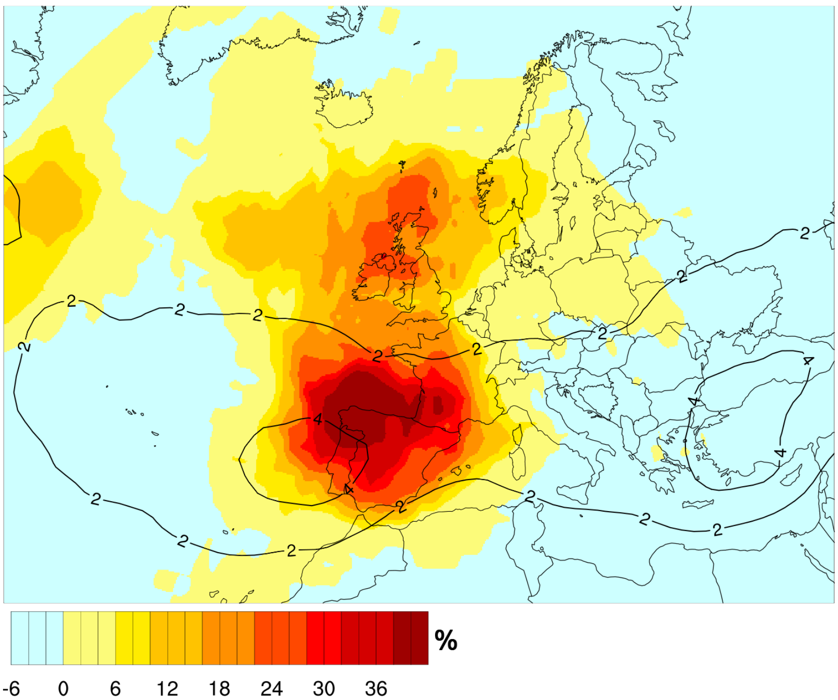

Figure 16. Climatological mean of cut-off low frequency (black contours; every 2 %; for May and June 1981 – 2010) and anomaly during the study period (shaded in % with reference to mean frequency in May and June; ERA-Interim)

.